Nonlinear Dyn (2025) 113:14265–14286
https://doi.org/10.1007/s11071-025-10902-0

RESEARCH

Spectral submanifolds in time delay systems

Bence Szaksz · Gábor Orosz · Gábor Stepan

Received: 16 April 2024 / Accepted: 14 January 2025 / Published online: 27 January 2025

Abstract The concept of spectral submanifolds, a powerful method of model order reduction of nonlinear systems, is extended to time delay systems that have infinite dimensional phase space representation. The proposed sun-star calculus based algorithm results in system reduction to manifolds which are constructed corresponding to either a real eigenvalue or to a pair of complex conjugate eigenvalues of the linearized system. Furthermore, it allows an improved approximation of self-excited oscillations exactly at the parameter point of interest, which could be further away from the corresponding Hopf bifurcation point. The paper includes case studies that demonstrate the capabilities of the algorithm.

Keywords Spectral submanifolds · Time delay · Model reduction · Sun-star calculus

Gábor Orosz and Gábor Stepan have contributed equally to this work.

B. Szaksz · G. Stepan
Department of Applied Mechanics, Faculty of Mechanical Engineering, Budapest University of Technology and Economics, Budapest 1111, Hungary
e-mail: stepan@mm.bme.hu

B. Szaksz (✉)
MTA-BME Lendulet "Momentum" Global Dynamics Research Group, Budapest University of Technology and Economics, Budapest 1111, Hungary
e-mail: szaksz@mm.bme.hu

G. Orosz
Department of Mechanical Engineering and Department of Civil and Environmental Engineering, University of Michigan, Ann Arbor, MI 48109, USA
e-mail: orosz@umich.edu

G. Stepan
HUN-REN–BME Dynamics of Machines Research Group, Budapest University of Technology and Economics, Budapest 1111, Hungary

1 Introduction

Linear spectral theory [1] is a powerful tool for the analysis of linear and linearizable dynamical systems. A system is linearizable when applying appropriate coordinate transformations, their equation of motion can be given in linear form. However, the analysis of essentially nonlinear systems requires more advanced techniques because of the lack of the superposition principle. Rosenberg introduced the concept of nonlinear normal modes [2] as the synchronous periodic oscillation of conservative systems, which was followed by further studies in the subsequent decades [3–5]. Later, Shaw and Pierre [6] extended this concept to dissipative systems inspired by the center manifold theory [7]. They defined the nonlinear normal mode as an invariant manifold that contains the stable equilibrium point of the system and it is tangent to the subspace spanned by the eigenvectors of the linearized system at that point.

In case of conservative systems, the Lyapunov subcenter-manifold theorem guarantees the existence of a unique and analytic invariant manifold under appropriate nonresonance conditions [8,9]. However,

these Shaw-Pierre-type surfaces are not unique [10]; generally, infinitely many of them correspond to a fixed point. Few years ago, Haller and Ponsioen [11] introduced the concept of spectral submanifolds (SSM) for dissipative systems, which is the unique smoothest nonlinear continuation of the spectral subspace of the linearized system. Their research is based on the mathematical background of Haro and de la Llave [12] and on the parametrization method of Cabré et al. [13–15] and Cirillo et al. [10].

Following the approach introduced by Haller, Szalai et al. [16] and Breunung et al. [17] applied this concept to generate backbone curves of forced vibrations, while Jain et al. [18] generalized the algorithm for high-dimensional finite element models. Furthermore, Ponsioen et al. [19] developed a MATLAB package for the automated computation of the SSMs, and Cenedese et al. [20] introduced a package for the data-driven modeling and prediction of dynamical behaviour based on Takens' delay-embedding theorem (see [16,21]). In the meantime, Vizzaccaro et al. [22] proposed an algorithm, in which they introduced the direct parametrization of invariant manifolds for model reduction in finite element models with the use of the left eigenvectors of large linearized systems. This algorithm was applied for micro-electromechanical structures (MEMS) by Opreni et al. [23]. Later, the method was also generalized for arbitrary order of expansion in [24,25]. Related technical difficulties are discussed in the review paper of Stoychev et al. [26] which describes the limitations of the different parametrizations of spectral submanifolds.

The above papers investigate the autonomous and/or non-autonomous dynamics of finite-dimensional systems, while to the best of the authors' knowledge, only two papers have been published in which infinite-dimensional SSM calculations were performed. Kogelbauer and Haller [27] investigated a damped-forced nonlinear beam model; they carried out a rigorous model reduction for the governing partial differential equation, the spectrum of which is given explicitly. Additionally, Buza [28] applied SSM theory to analyze the dynamics of the Navier-Stokes equations.

In this paper, we focus on delay-differential equations (DDEs), which also have an infinite-dimensional phase space representation [29,30]. A wide variety of methods are proposed for the finite-dimensional approximation of DDEs including the shift operator induced approach of Mäkilä and Partington [31], the semidiscretization, introduced by Insperger and Stepan [32], or the Krylov based model reduction of Michiels et al. [33]. The discretization is a useful tool for the approximation of invariant manifolds of time delay systems (see the work of Farkas [34] and Sahai et al. [35]). However, a subsequent model reduction may already lose the infinite dimensional nature of the original system. The papers of Jarlebring et al. [36], and van de Wouw et al. [37] keep the infinite dimensional nature of the reduced dynamics, while reducing the order of the original DDE; furthermore, Scarciotti et al. [38] utilize the moment matching for the model reduction of DDEs. Finally, it must be mentioned that Groothedde and James [39] introduced a parametrization method for unstable manifolds of DDEs based on the work of He and de la Llave [40,41]. Their approach is closely related to the aforementioned spectral submanifolds, however, they assume only a linear reduced dynamics.

Here, we extend the concept of spectral submanifolds for time delay systems. During the calculations, we apply the dual perturbation framework (sun-star calculus) developed by Clement et al. [42,43], and the corresponding results of Diekmann et al. [44] and Wage [45]. The obtained reduced dynamics are of finite dimension, while the infinite dimensional nature of the original system is preserved in the manifold itself as opposed to the discretization methods used for DDEs. The proposed method enables us to execute the manifold calculations analytically, and accurately capture the essential finite-dimensional dynamics.

The obtained results may be beneficial in a series of time delay systems subjected to relevant nonlinearities. Examples include machine tool vibrations [46–48], wheel shimmy [49,50], robot control [51–53], human balance [54–56], and traffic dynamics [57,58], to mention a few.

The paper is organized as follows. After the problem statement in Sect. 2, the theoretical background of the sun-star calculus is summarized in Sect. 3. This section also contains the framework for the treatment of the nonlinearities. Section 4 presents the derivation of spectral submanifolds for time delay systems. First, we carry out a projection to the manifold corresponding to a real eigenvalue, which is followed by a projection to the manifold corresponding to a pair of complex conjugate eigenvalues. After the theoretical calculations, Sect. 5 discusses the SSM calculation for the simplest nontrivial scalar nonlinear DDE. The SSM and the corresponding reduced dynamics are calculated

both in case of a real dominant eigenvalue and in case of a dominant pair of complex conjugate eigenvalues. Finally, Sect. 6 presents concluding remarks and future research directions.

2 Problem statement

Let us consider a smooth nonlinear delay dynamical system with the state vector $\mathbf{x} \in \mathbb{R}^n$ and constant time delay $\tau \in \mathbb{R}$, which is governed by the delay-differential equation (DDE)

$$\dot{\mathbf{x}}(t) = \mathbf{L}\mathbf{x}(t) + \mathbf{R}\mathbf{x}(t-\tau) + \mathbf{N}(\mathbf{x}(t), \mathbf{x}(t-\tau)). \quad (1)$$

Here, dot denotes the time derivative, $\mathbf{L} \in \mathbb{R}^{n\times n}$ and $\mathbf{R} \in \mathbb{R}^{n\times n}$ are the coefficient matrices of the actual and the delayed states, respectively, while the continuously differentiable function $\mathbf{N} : \mathbb{R}^n \times \mathbb{R}^n \to \mathbb{R}^n$ contains the nonlinear terms with zero as trivial solution.

Consider a stable case, that is, all the eigenvalues of the linearized system have negative real parts. We assume that the slow dynamics is determined either by a rightmost real eigenvalue or a rightmost pair of slightly damped complex conjugate eigenvalues. The goal of the current study is to calculate the SSM and the reduced dynamics corresponding to the dominant eigenvalue(s).

Note that although, the spectrum of DDEs cannot be expressed in closed form, there are several well developed methods for the solution of the quasi-polynomial characteristic equation, for example, the contour integration based method [59] or the quasi-polynomial root finder [60]. Other algorithms are based on the discretization of the DDE, which can be followed by a Newton iteration in the original characteristic equation [32,61–64]. In this study, we assume that the dominant eigenvalues are known, or at least well approximated.

3 Sun-star calculus

Let us rewrite the DDE (1) as the equivalent operator differential equation (OpDE)

$$\dot{\mathbf{x}}_t(\vartheta) = \mathcal{A}^{\odot\star}\mathbf{x}_t(\vartheta) + \mathcal{N}(\mathbf{x}_t(\vartheta)), \quad (2)$$

where the state vector

$$\mathbf{x}_t(\vartheta) = \mathbf{x}(t+\vartheta), \ \vartheta \in [-\tau, 0], \quad (3)$$

is defined in the Banach space $\mathcal{B} = \mathcal{C}([-\tau, 0], \mathbb{C}^n)$, the linear operator $\mathcal{A}^{\odot\star} : \mathcal{B} \to \mathcal{B}$ assumes the form

$$\mathcal{A}^{\odot\star}\Phi = \begin{cases} \frac{\mathrm{d}\Phi}{\mathrm{d}\vartheta}(\vartheta), & \text{if } \vartheta \in [-\tau, 0), \\ \mathbf{L}\Phi(0) + \mathbf{R}\Phi(-\tau), & \text{if } \vartheta = 0, \end{cases} \quad (4)$$

for $\Phi \in \mathcal{B}$, while the nonlinear operator $\mathcal{N} : \mathcal{B} \to \mathcal{B}$ is obtained as

$$\mathcal{N}(\Phi) = \begin{cases} \mathbf{0}, & \text{if } \vartheta \in [-\tau, 0), \\ \mathbf{N}(\Phi(0), \Phi(-\tau)), & \text{if } \vartheta = 0. \end{cases} \quad (5)$$

Note that $\star$ (star) denotes the adjoint, while $\odot$ (sun) denotes the adjoint in a restricted domain to be defined later.

The characteristic matrix corresponding to the DDE (1) is

$$\Delta(\lambda) = \lambda\mathbf{I} - \mathbf{L} - \mathbf{R}\mathrm{e}^{-\lambda\tau}, \quad (6)$$

which leads to the characteristic equation

$$\det(\Delta(\lambda)) = 0. \quad (7)$$

This is a transcendental equation that has got infinitely many roots, from which only finitely many are located to the right of a vertical line in the complex plane. This allows the projection of the dynamics to a selected finite dimensional subspace. These characteristic roots are exactly the same as the eigenvalues of the linear operator $\mathcal{A}^{\odot\star}$.

The eigenfunction $\mathbf{s} \in \mathcal{B}$ of the operator $\mathcal{A}^{\odot\star}$ corresponding to an eigenvalue λ is defined by

$$\mathcal{A}^{\odot\star}\mathbf{s} = \lambda\mathbf{s}. \quad (8)$$

This leads to a boundary value problem, the solution of which is

$$\mathbf{s}(\vartheta) = \mathbf{q}\mathrm{e}^{\lambda\vartheta}, \quad (9)$$

where $\mathbf{q} \in \mathbb{C}^n$ spans the nullspace of $\Delta(\lambda)$; it is obtained from

$$\Delta(\lambda)\mathbf{q} = \mathbf{0}. \quad (10)$$

Note that $\mathbf{q}$ is defined up to a scalar multiplier.

In order to carry out projections to a particular spectral subspace, the adjoint operator $\mathcal{A}^{\odot} : \mathcal{D}(\mathcal{A}^{\odot}) \subset \mathcal{B}^{\star} \to \mathcal{B}^{\star}$ should also be introduced. This acts on the dual space $\mathcal{B}^{\star} = \mathrm{NBV}([0, \tau], \mathbb{C}^n)$, where NBV refers to normalized bounded variation. The operator assumes the form:

$$\mathcal{A}^{\odot}\Psi = \begin{cases} \frac{\mathrm{d}\Psi}{\mathrm{d}\sigma}(0), & \text{if } \sigma = 0, \\ \frac{\mathrm{d}\Psi}{\mathrm{d}\sigma}(\sigma) + \Psi(0)\mathbf{L}, & \text{if } \sigma \in (0, \tau), \\ \Psi(0)(\mathbf{L} + \mathbf{R}), & \text{if } \sigma = \tau, \end{cases} \quad (11)$$

where $\Psi \in \mathcal{B}^\star$ and $\Psi(0)$ is a row vector. The domain of the operator $\mathcal{A}^\odot$ is restricted to

$$\mathcal{D}(\mathcal{A}^\odot) = \left\{ \Psi \in \mathcal{B}^\star : \frac{\mathrm{d}\Psi}{\mathrm{d}\sigma}(\tau) = \mathbf{0} \right\}. \tag{12}$$

The corresponding derivation is presented in Appendix A.1.

Utilizing this domain restriction, the operators $\mathcal{A}^\odot$ and $\mathcal{A}^{\odot\star}$ are adjoint to each other with respect to the pairing

$$\langle \Psi, \Phi \rangle = \Psi(0)\Phi(0) + \int_0^\tau \frac{\mathrm{d}\Psi}{\mathrm{d}\theta}(\theta)\Phi(-\theta)\mathrm{d}\theta, \tag{13}$$

that is,

$$\langle \mathcal{A}^\odot \Psi, \Phi \rangle = \langle \Psi, \mathcal{A}^{\odot\star} \Phi \rangle. \tag{14}$$

Again, the eigenvalues of $\mathcal{A}^\odot$ are the same as the characteristic roots of the DDE (1), and its eigenfunctions satisfy

$$\mathcal{A}^\odot \mathbf{n} = \lambda \mathbf{n}. \tag{15}$$

Appendix A presents the detailed derivation of the solution of (15) assuming continuous extension at $\lambda = 0$, which yields

$$\mathbf{n}(\sigma) = \begin{cases} \mathbf{p}\mathrm{e}^{\lambda\sigma}, & \text{if } \sigma \le 0, \\ \mathbf{p}\left(\mathbf{I} + \mathbf{R}\mathrm{e}^{-\lambda\tau}\frac{\mathrm{e}^{\lambda\sigma}-1}{\lambda}\right), & \text{if } \sigma \in (0,\tau), \\ \mathbf{p}\left(\mathbf{I} + \mathbf{R}\mathrm{e}^{-\lambda\tau}\frac{\mathrm{e}^{\lambda\tau}-1}{\lambda}\right), & \text{if } \sigma \ge \tau, \end{cases} \tag{16}$$

where the row vector $\mathbf{p} \in \mathbb{C}^n$ is the solution of

$$\mathbf{p}\Delta(\lambda) = \mathbf{0}. \tag{17}$$

Note that $\mathbf{n}(\sigma)$ in (16) satisfies the domain restriction (12) at $\sigma = \tau$.

Equation (17) allows us to choose one coordinate of $\mathbf{p}$ freely, which otherwise has to satisfy the normalization

$$\langle \mathbf{n}, \mathbf{s} \rangle = 1. \tag{18}$$

After some algebraic manipulation, the normalization assumes the form

$$\mathbf{p}\Delta'(\lambda)\mathbf{q} = 1, \tag{19}$$

where prime denotes the derivative with respect to λ.

In general, the projection of a solution $\mathbf{x}_t$ to an eigenfunction $\mathbf{s}_j$ yields the corresponding coordinate

$$\begin{aligned} y_j(t) &= \langle \mathbf{n}_j, \mathbf{x}_t \rangle \\ &= \mathbf{p}_j \left(\mathbf{x}(t) + \int_{-\tau}^0 \mathbf{R}\mathrm{e}^{-\lambda_j(\vartheta+\tau)} \mathbf{x}(t+\vartheta)\mathrm{d}\vartheta \right). \end{aligned} \tag{20}$$

Note that here, the integration variable is changed in the pairing (13) with $\vartheta = -\theta$.

Selecting the K rightmost characteristic roots, the state can be decomposed as

$$\mathbf{x}_t(\vartheta) = \sum_{j=1}^K y_j(t)\mathbf{s}_j(\vartheta) + \mathbf{e}(t,\vartheta), \tag{21}$$

where the term $|\mathbf{e}(t,\vartheta)|$ decreases as K is increased.

Following [23,45,65], let us divide the nonlinearity in (2) into second, third, and higher-order terms:

$$\mathcal{N}(\Phi) = \frac{1}{2!}\mathbf{B}(\Phi,\Phi) + \frac{1}{3!}\mathbf{C}(\Phi,\Phi,\Phi) + (||\Phi||^4), \tag{22}$$

where

$$\mathbf{B}(\Phi,\Lambda) = \begin{cases} \mathbf{0}, & \text{if } \vartheta \in [-\tau, 0), \\ \mathbf{b}(\Phi,\Lambda), & \text{if } \vartheta = 0, \end{cases} \tag{23}$$

$$\mathbf{C}(\Phi,\Lambda,\Gamma) = \begin{cases} \mathbf{0}, & \text{if } \vartheta \in [-\tau, 0), \\ \mathbf{c}(\Phi,\Lambda,\Gamma), & \text{if } \vartheta = 0. \end{cases} \tag{24}$$

Here $\mathbf{b}(\Phi,\Lambda)$ and $\mathbf{c}(\Phi,\Lambda,\Gamma)$ are symmetric multilinear vector functions of $\Phi, \Lambda, \Gamma \in \mathcal{B}$; their coordinates take the form

$$b_i(\Phi,\Lambda) = \sum_{j,k=1}^{2n} \frac{\partial^2 N_i}{\partial\tilde{x}_j \partial\tilde{x}_k}\bigg|_{\tilde{\mathbf{x}}=\mathbf{0}} \tilde{\Phi}_j \tilde{\Lambda}_k, \tag{25}$$

$$c_i(\Phi,\Lambda,\Gamma) = \sum_{j,k,l=1}^{2n} \frac{\partial^3 N_i}{\partial\tilde{x}_j \partial\tilde{x}_k \partial\tilde{x}_l}\bigg|_{\tilde{\mathbf{x}}=\mathbf{0}} \tilde{\Phi}_j \tilde{\Lambda}_k \tilde{\Gamma}_l, \tag{26}$$

for $i = 1, 2, \ldots, n$. Furthermore, tilde refers to the $2n$-dimensional vectors

$$\tilde{\Phi} = \begin{bmatrix} \Phi(0) \\ \Phi(-\tau) \end{bmatrix}, \quad \tilde{\Lambda} = \begin{bmatrix} \Lambda(0) \\ \Lambda(-\tau) \end{bmatrix}, \quad \tilde{\Gamma} = \begin{bmatrix} \Gamma(0) \\ \Gamma(-\tau) \end{bmatrix}, \tag{27}$$

and to the corresponding extended state vector

$$\tilde{\mathbf{x}}(t) = \begin{bmatrix} \mathbf{x}(t) \\ \mathbf{x}(t-\tau) \end{bmatrix}. \tag{28}$$

This extension allows us to handle both delay-free, delayed, and combined terms in the nonlinearity. In practical examples, the nonlinearity is often purely delay-free or purely delayed; in these cases, the expressions (27) and (28) are simplified accordingly.

4 Spectral submanifold for delay differential equations

Overlooking the special cases of multiple roots, the dominant dynamics of system (1) is determined either by a real root or by a pair of complex conjugate roots. This section presents the calculation of the corresponding one- or two-dimensional reduced dynamics and the construction of the spectral submanifolds.

4.1 Projection to the manifold corresponding to a dominant real eigenvalue

Let us assume that λ_1 is the real dominant eigenvalue of the system (1), i.e., it satisfies the characteristic equation (7), while $\mathbf{s}(\vartheta)$ and $\mathbf{n}(\sigma)$ are the corresponding eigenfunctions, cf. (9) and (16). Then, the corresponding spectral submanifold (SSM) can be searched in the form

$$\begin{aligned}\mathbf{W}(z;\vartheta) =&\mathbf{W}_1(\vartheta)z+\frac{1}{2}\mathbf{W}_2(\vartheta)z^2\\ &+\frac{1}{6}\mathbf{W}_3(\vartheta)z^3+\mathcal{O}(z^4),\end{aligned} \tag{29}$$

where z is called the parametrization variable. The dynamics on the SSM, that is, the reduced dynamics assumes the form

$$\dot{z}=\lambda_1 z+\beta_2 z^2+\beta_3 z^3. \tag{30}$$

Note that, here, we assume a so-called graph-style parametrization [18] of the reduced dynamics, that is, all the powers of the variable z appear in the right-hand side of (30). If one would like to obtain a pitchfork or a transcritical bifurcation type reduced dynamics, then, accordingly, either β_2 or β_3 should be neglected in the following calculations, respectively.

Substitution of $\mathbf{x}_t(\vartheta)=\mathbf{W}(z(t);\vartheta)$ into the OpDE (2) leads to the homological equation [65]

$$\frac{\partial\mathbf{W}(z;\vartheta)}{\partial z}\dot{z}=\mathcal{A}^{\odot\star}\mathbf{W}(z;\vartheta)+\mathcal{N}(\mathbf{W}(z;\vartheta)). \tag{31}$$

Using (22), (29) and (30), the expansion of the left- and right-hand sides yields

$$\begin{aligned}&\lambda_1\mathbf{W}_1z+\lambda_1\mathbf{W}_2z^2+\beta_2\mathbf{W}_1z^2+\frac{1}{2}\lambda_1\mathbf{W}_3z^3\\ &+\beta_2\mathbf{W}_2z^3+\beta_3\mathbf{W}_1z^3+\mathcal{O}(z^4)\\ &=\mathcal{A}^{\odot\star}\mathbf{W}_1z+\frac{1}{2}\mathcal{A}^{\odot\star}\mathbf{W}_2z^2+\frac{1}{6}\mathcal{A}^{\odot\star}\mathbf{W}_3z^3\\ &+\frac{1}{2}\mathbf{B}(\mathbf{W}_1,\mathbf{W}_1)z^2+\frac{1}{2}\mathbf{B}(\mathbf{W}_1,\mathbf{W}_2)z^3\\ &+\frac{1}{6}\mathbf{C}(\mathbf{W}_1,\mathbf{W}_1,\mathbf{W}_1)z^3+\mathcal{O}(z^4).\end{aligned} \tag{32}$$

The manifold is determined by balancing the coefficients of equal powers in z.

In case of z^1, this yields

$$\lambda_1\mathbf{W}_1=\mathcal{A}^{\odot\star}\mathbf{W}_1, \tag{33}$$

thus, $\mathbf{W}_1(\vartheta)$ is the eigenfunction of the operator $\mathcal{A}^{\odot\star}$ corresponding to the dominant root λ_1 (cf. (8)), that is,

$$\mathbf{W}_1(\vartheta)=\mathbf{s}(\vartheta). \tag{34}$$

Utilizing (34), the coefficients of z^2 satisfy

$$(2\lambda_1\mathcal{I}-\mathcal{A}^{\odot\star})\mathbf{W}_2=\mathbf{B}(\mathbf{s},\mathbf{s})-2\beta_2\mathbf{s}. \tag{35}$$

In order to satisfy the normality condition $\langle\mathbf{n},\mathbf{W}_2\rangle=0$, the term $2\beta_2\mathbf{s}$ has to balance the second order nonlinearities in the direction of the eigenfunction $\mathbf{s}$. Thus, pairing (35) with $\mathbf{n}$ and using (23) yield

$$\beta_2=\frac{1}{2}\mathbf{pb}(\mathbf{s},\mathbf{s}). \tag{36}$$

Similarly, balancing the coefficients of z^3 leads to

$$\begin{aligned}(3\lambda_1\mathcal{I}-\mathcal{A}^{\odot\star})\mathbf{W}_3 =&3\mathbf{B}(\mathbf{s},\mathbf{W}_2)+\mathbf{C}(\mathbf{s},\mathbf{s},\mathbf{s})\\ &-6\beta_2\mathbf{W}_2-6\beta_3\mathbf{s},\end{aligned} \tag{37}$$

while considering $\langle\mathbf{n},\mathbf{W}_3\rangle=0$, pairing (37) with $\mathbf{n}$, and using (23),(24) imply

$$\beta_3=\frac{1}{6}\mathbf{p}(3\mathbf{b}(\mathbf{s},\mathbf{W}_2)+\mathbf{c}(\mathbf{s},\mathbf{s},\mathbf{s})). \tag{38}$$

As the coefficients of the reduced order dynamics are already known, one can solve the boundary value problems (35) and (37) under certain non-resonance conditions. Since the power series expansion of the SSM can be continued to any order, these non-resonance conditions take the form

$$\mathrm{Ker}(k\lambda_1\mathcal{I}-\mathcal{A}^{\odot\star})\neq\{0\},\quad k=2,3,\dots, \tag{39}$$

where the identity operator is denoted by $\mathcal{I}$.

Note that according to the finite dimensional SSM theory, the non-resonance conditions must hold up to any order for the SSM to be analytic [11,13]. If the ratio of the leftmost and rightmost eigenvalues is a finite number, then only finitely many non-resonance conditions should be checked. This was utilized in [27] as well, where the authors derived the infinite dimensional SSM of a partial differential equation. In that case, a special type of damping had to be applied, at which there is a lower bound for the radius of the characteristic multipliers. They could express these characteristic multipliers in closed form, and then, the finitely many relevant non-resonance conditions could be investigated.

In the case of delay differential equations, there are infinitely many eigenvalues, the real part of which tend to minus infinity; moreover, the eigenvalues cannot be expressed in closed form. Therefore, proving that the non-resonance conditions fulfill is possible only in some special cases, one of which is the one dimensional SSM of the scalar case study in Sect. 5.1. Unfortunately, we could not prove the existence and uniqueness of the delayed SSMs in general. In the followings, we assume that the non-resonance conditions fulfill.

The solution of the boundary value problems (35) and (37) yields

$$\mathbf{W}_2(\vartheta) = \Delta^{-1}(2\lambda_1)\mathbf{b}(\mathbf{s},\mathbf{s})\mathrm{e}^{2\lambda_1\vartheta} - 2\frac{\beta_2}{\lambda_1}\mathbf{q}\mathrm{e}^{\lambda_1\vartheta}, \tag{40}$$

$$\begin{aligned}\mathbf{W}_3(\vartheta) = {} & \Delta^{-1}(3\lambda_1)(3\mathbf{b}(\mathbf{s},\mathbf{W}_2) \\ & + \mathbf{c}(\mathbf{s},\mathbf{s},\mathbf{s}))\mathrm{e}^{3\lambda_1\vartheta} \\ & + 6\frac{\beta_2}{\lambda_1}\Delta^{-1}(3\lambda_1)\mathbf{b}(\mathbf{s},\mathbf{s})\mathrm{e}^{3\lambda_1\vartheta} \\ & - 6\frac{\beta_2}{\lambda_1}\Delta^{-1}(2\lambda_1)\mathbf{b}(\mathbf{s},\mathbf{s})\mathrm{e}^{2\lambda_1\vartheta} \\ & + \left(6\frac{\beta_2^2}{\lambda_1^2} - 3\frac{\beta_3}{\lambda_1}\right)\mathbf{q}\mathrm{e}^{\lambda_1\vartheta},\end{aligned} \tag{41}$$

see Appendix C for the detailed derivation.

Finally, substituting (34), (40) and (41) into (29) provides the SSM. If the manifold is obtained corresponding to a dominant stable eigenvalue $\lambda_1 < 0$ in (1), the trajectories tend to this manifold and stay close to it as they approach the stable equilibrium point.

The projection of the manifold to the eigenfunction $\mathbf{s}(\vartheta)$ yields the coordinate

$$y(z) = \langle \mathbf{n}, \mathbf{W}(z)\rangle = z, \tag{42}$$

while the part of the SSM, which is orthogonal to $\mathbf{s}(\vartheta)$, assumes the form

$$\mathbf{w}(z;\vartheta) = \mathbf{W}(z;\vartheta) - y(z)\mathbf{s}(\vartheta), \tag{43}$$

that is,

$$\mathbf{w}(z;\vartheta) = \frac{1}{2}\mathbf{W}_2(\vartheta)z^2 + \frac{1}{6}\mathbf{W}_3(\vartheta)z^3 + \mathcal{O}(z^4). \tag{44}$$

Figure 1 presents an example for the visualization of the SSM when $\lambda_1 < 0$. The horizontal axis represents the eigendirection corresponding to $\mathbf{s}$, the coordinate along which is $y(z) = z$. The brown curve presents the nonlinear part of the SSM at $\vartheta = 0$, while the green curve is a particular trajectory transformed to this space

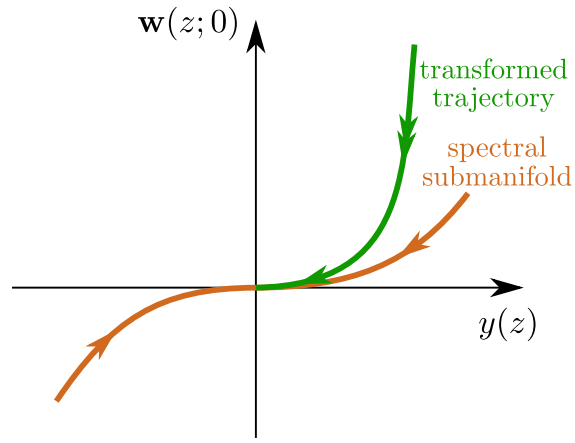

Fig. 1 Schematic diagram illustrating the convergence of a trajectory towards the spectral submanifold corresponding to a real dominant negative root. The brown curve is the part of the spectral submanifold, which is orthogonal to the dominant eigenfunction, while the green curve refers to the trajectory transformed to the same space. Note that $y(z) = z$

(see details in Appendix D). As it can be observed, the trajectory first approaches the SSM. The dynamics close to the SSM can be approximated with the reduced dynamics (30).

Note that if a pitchfork-type bifurcation is assumed in the reduced dynamics, that is, the coefficient β_2 is zero, then the pairing $\langle \mathbf{n}, \mathbf{W}_2\rangle$ may not be zero in case of nonsymmetric nonlinearities with $\mathbf{B}(\mathbf{s},\mathbf{s}) \neq \mathbf{0}$. In these cases, the coordinate y can be introduced in the form

$$y(z) = z + \frac{1}{2}\langle \mathbf{n}, \mathbf{W}_2\rangle z^2, \tag{45}$$

along the eigenfunction $\mathbf{s}$ and this will appear also in (43).

4.2 Projection to the manifold corresponding to a pair of complex conjugate eigenvalues

In some critical engineering applications, the time delay system is slightly damped, in which case a pair of complex conjugate roots is responsible for the slow dynamics. This section presents the derivation of the corresponding SSM.

Assume that λ_1 and $\lambda_2 = \overline{\lambda}_1$ form a pair of dominant eigenvalues, i.e., they satisfy the characteristic equation (7), while the corresponding eigenfunctions are $\mathbf{s}(\vartheta)$, $\mathbf{n}(\sigma)$ and $\overline{\mathbf{s}}(\vartheta)$, $\overline{\mathbf{n}}(\sigma)$, respectively, see (9) and (16).

In this case, the SSM assumes the form

$$\begin{aligned}\mathbf{W}(z,\bar{z};\vartheta) = \mathbf{W}_{10}(\vartheta)z \quad &+ \mathbf{W}_{01}(\vartheta)\bar{z} \\ &+ \frac{1}{2}\mathbf{W}_{20}(\vartheta)z^2 + \mathbf{W}_{11}(\vartheta)z\bar{z} \\ &+ \frac{1}{2}\mathbf{W}_{02}(\vartheta)\bar{z}^2 \\ &+ \frac{1}{6}\mathbf{W}_{30}(\vartheta)z^3 + \frac{1}{2}\mathbf{W}_{21}(\vartheta)z^2\bar{z} \\ &+ \frac{1}{2}\mathbf{W}_{12}(\vartheta)z\bar{z}^2 + \frac{1}{6}\mathbf{W}_{03}(\vartheta)\bar{z}^3 + (|z|^4),\end{aligned} \tag{46}$$

while the reduced dynamics is governed by the normal form

$$\begin{bmatrix}\dot{z}\\ \dot{\bar{z}}\end{bmatrix} = \begin{bmatrix}\lambda_1 z + \beta_{21} z^2\bar{z}\\ \bar{\lambda}_1\bar{z} + \bar{\beta}_{21} z\bar{z}^2\end{bmatrix}. \tag{47}$$

Note that the algorithm is also able to handle the graph-style parametrization of the normal form, where all the monomials of z and $\bar{z}$ appear. However, this leads to a lot of unknown coefficients and lengthy algebraic expressions. Here, we calculate the reduced dynamics directly in normal form including the minimal number of monomials, which allows us to obtain simple and direct expressions for the arising limit cycles.

Substituting $\mathbf{x}_t(\vartheta) = \mathbf{W}(z(t),\bar{z}(t);\vartheta)$ into the OpDE (2) yields the homological equation

$$\begin{aligned}&\frac{\partial \mathbf{W}(z,\bar{z};\vartheta)}{\partial z}\dot{z} + \frac{\partial \mathbf{W}(z,\bar{z};\vartheta)}{\partial \bar{z}}\dot{\bar{z}} \\ &= \mathcal{A}^{\odot\star}\mathbf{W}(z,\bar{z};\vartheta) + \mathcal{N}(\mathbf{W}(z,\bar{z};\vartheta));\end{aligned} \tag{48}$$

Appendix B presents this homological equation in an expanded form after the substitution of (46) and (47). Again, the coefficients of the SSM are determined by balancing the terms with the same powers of z and $\bar{z}$.

Balancing the coefficients of z^1, one obtains

$$\lambda_1\mathbf{W}_{10} = \mathcal{A}^{\odot\star}\mathbf{W}_{10}, \tag{49}$$

thus,

$$\mathbf{W}_{10}(\vartheta) = \mathbf{s}(\vartheta), \tag{50}$$

cf. (8). Similarly, the $\bar{z}^1$ terms lead to $\mathbf{W}_{01}(\vartheta) = \bar{\mathbf{s}}(\vartheta)$, that is, $\mathbf{W}_{01}(\vartheta) = \overline{\mathbf{W}}_{10}(\vartheta)$. Furthermore, balancing z^2, $z\bar{z}$, z^3, $z^2\bar{z}$ yields

$$(2\lambda_1\mathcal{I} - \mathcal{A}^{\odot\star})\mathbf{W}_{20} = \mathbf{B}(\mathbf{s},\mathbf{s}), \tag{51}$$

$$((\lambda_1+\bar{\lambda}_1)\mathcal{I} - \mathcal{A}^{\odot\star})\mathbf{W}_{11} = \mathbf{B}(\mathbf{s},\bar{\mathbf{s}}), \tag{52}$$

$$\begin{aligned}(3\lambda_1\mathcal{I} - \mathcal{A}^{\odot\star})\mathbf{W}_{30} &= 3\mathbf{B}(\mathbf{s},\mathbf{W}_{20}) \\ &\quad + \mathbf{C}(\mathbf{s},\mathbf{s},\mathbf{s}),\end{aligned} \tag{53}$$

$$\begin{aligned}((2\lambda_1+\bar{\lambda}_1)\mathcal{I} - \mathcal{A}^{\odot\star})\mathbf{W}_{21} &= 2\mathbf{B}(\mathbf{s},\mathbf{W}_{11}) + \mathbf{B}(\bar{\mathbf{s}},\mathbf{W}_{20}) \\ &\quad + \mathbf{C}(\bar{\mathbf{s}},\mathbf{s},\mathbf{s}) - 2\beta_{21}\mathbf{s},\end{aligned} \tag{54}$$

respectively. Due to the selection of the normal form (47), we consider that

$$\langle \mathbf{n}, \mathbf{W}_{21}\rangle = 0; \tag{55}$$

then, the pairing of $\mathbf{n}(\sigma)$ with (54) and using (23),(24) yield that

$$\beta_{21} = \frac{1}{2}\mathbf{p}(\mathbf{b}(\bar{\mathbf{s}},\mathbf{W}_{20}) + 2\mathbf{b}(\mathbf{s},\mathbf{W}_{11}) + \mathbf{c}(\bar{\mathbf{s}},\mathbf{s},\mathbf{s})). \tag{56}$$

Finally, Eqs. (51)–(54) lead to boundary value problems, the solutions of which are

$$\mathbf{W}_{20}(\vartheta) = \Delta^{-1}(2\lambda_1)\mathbf{b}(\mathbf{s},\mathbf{s})\mathrm{e}^{2\lambda_1\vartheta}, \tag{57}$$

$$\mathbf{W}_{11}(\vartheta) = \Delta^{-1}(\lambda_1+\bar{\lambda}_1)\mathbf{b}(\mathbf{s},\bar{\mathbf{s}})\mathrm{e}^{(\lambda_1+\bar{\lambda}_1)\vartheta}, \tag{58}$$

$$\mathbf{W}_{30}(\vartheta) = \Delta^{-1}(3\lambda_1)[3\mathbf{b}(\mathbf{s},\mathbf{W}_{20}) + \mathbf{c}(\mathbf{s},\mathbf{s},\mathbf{s})]\mathrm{e}^{3\lambda_1\vartheta}, \tag{59}$$

$$\begin{aligned}\mathbf{W}_{21}(\vartheta) = \Delta^{-1}(2\lambda_1+\bar{\lambda}_1)&[\mathbf{b}(\bar{\mathbf{s}},\mathbf{W}_{20}) + 2\mathbf{b}(\mathbf{s},\mathbf{W}_{11}) \\ &+ \mathbf{c}(\bar{\mathbf{s}},\mathbf{s},\mathbf{s})]\mathrm{e}^{(2\lambda_1+\bar{\lambda}_1)\vartheta} - \frac{2\beta_{21}}{\lambda_1+\bar{\lambda}_1}\mathbf{q}\mathrm{e}^{\lambda_1\vartheta}.\end{aligned} \tag{60}$$

see Appendix C. As the inverse Δ^{-1} of the characteristic matrix implies, in this case, the non-resonance conditions take the form

$$\begin{aligned}&\mathrm{Ker}((k\lambda_1 + l\bar{\lambda}_1)\mathcal{I} - \mathcal{A}^{\odot\star}) \neq \{0\}, \\ &k + l = 2, 3, \ldots.\end{aligned} \tag{61}$$

The further coefficients are obtained as $\mathbf{W}_{02}(\vartheta) = \overline{\mathbf{W}}_{20}(\vartheta)$, $\mathbf{W}_{03}(\vartheta) = \overline{\mathbf{W}}_{30}(\vartheta)$ and $\mathbf{W}_{12}(\vartheta) = \overline{\mathbf{W}}_{21}(\vartheta)$. This implies that the imaginary parts in (46) cancel out each other and so the spectral submanifold is real; this is in accordance with the requirement that the solution of the dynamical system (1) should be real. Moreover, the real coefficient $\mathbf{W}_{11}(\vartheta)$ is responsible for the shift in the mean value of the large amplitude oscillations, which is well-known in the presence of second (or more generally, even) order nonlinearities.

Let $y(z,\bar{z}) = \langle \mathbf{n}, \mathbf{W}(z,\bar{z})\rangle$ denote the coordinate of the SSM along the eigenfunction $\mathbf{s}(\vartheta)$, which leads to the near-identity transformation

$$\begin{aligned}y(z,\bar{z}) = z &+ \frac{1}{2}\langle \mathbf{n},\mathbf{W}_{20}\rangle z^2 + \langle \mathbf{n},\mathbf{W}_{11}\rangle z\bar{z} \\ &+ \frac{1}{2}\langle \mathbf{n},\mathbf{W}_{02}\rangle \bar{z}^2 + \frac{1}{6}\langle \mathbf{n},\mathbf{W}_{30}\rangle z^3 \\ &+ \frac{1}{2}\langle \mathbf{n},\mathbf{W}_{12}\rangle z\bar{z}^2 + \frac{1}{6}\langle \mathbf{n},\mathbf{W}_{03}\rangle \bar{z}^3 \\ &+ (|z|^4).\end{aligned} \tag{62}$$

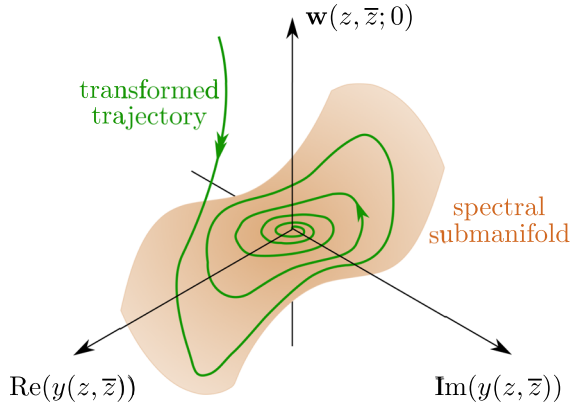

Fig. 2 Schematic diagram illustrating the convergence of a trajectory towards the spectral submanifold corresponding to a pair of complex conjugate dominant roots with negative real part. The brown surface is that part of the spectral submanifold, which is orthogonal to the dominant eigenfunctions, while the green curve refers to the trajectory transformed to the same space

Here, the $\langle \mathbf{n}, \mathbf{W}_{21} \rangle$ term is missing, since it equals to zero (see (55)).

Thus, the part of the SSM which is orthogonal to the space spanned by the eigenfunctions $\mathbf{s}(\vartheta)$ and $\overline{\mathbf{s}}(\vartheta)$, assumes the form:

$$\begin{aligned}\mathbf{w}(z,\overline{z};\vartheta) &= \mathbf{W}(z,\overline{z};\vartheta) - y(z,\overline{z})\mathbf{s}(\vartheta) \\ &\quad -\overline{y}(z,\overline{z})\overline{\mathbf{s}}(\vartheta).\end{aligned} \tag{63}$$

Figure 2 presents a schematic diagram of the spectral submanifold and a particular trajectory considering a stable case with $\mathrm{Re}\lambda_{1,2} < 0$. The brown surface represents the SSM above the space spanned by the real and imaginary parts of the eigenfunction $\mathbf{s}(\vartheta)$; the green curve is a particular trajectory, which first tends to the SSM, then it spirals towards the fixed point staying close to the SSM.

A valuable outcome of the spectral projection is, that it allows the direct approximation of the self-excited oscillations exactly at the parameter point of interest, which might be far from a related Hopf bifurcation. Let us consider the first row of the reduced dynamics (47), and look for the solution in the form

$$z(t) = \rho(t)\mathrm{e}^{\mathrm{i}\alpha(t)}, \tag{64}$$

which yields

$$\dot{\rho}(t) + \mathrm{i}\dot{\alpha}(t)\rho(t) = \lambda_1\rho(t) + \beta_{21}\rho^3(t). \tag{65}$$

Separating the real and imaginary parts results

$$\dot{\rho}(t) = \mathrm{Re}\lambda_1\rho(t) + \mathrm{Re}\beta_{21}\rho^3(t)\,, \tag{66}$$

$$\dot{\alpha}(t)\rho(t) = \mathrm{Im}\lambda_1\rho(t) + \mathrm{Im}\beta_{21}\rho^3(t)\,. \tag{67}$$

In case of a steady state periodic motion, we have $\dot{\rho} = 0$ and $\alpha = \omega t$, which imply that there exists a limit cycle if the following inequality holds:

$$\frac{\mathrm{Re}\lambda_1}{\mathrm{Re}\beta_{21}} < 0. \tag{68}$$

The corresponding self-excited oscillation is unstable for $\mathrm{Re}\lambda_1 < 0$ and stable for $\mathrm{Re}\lambda_1 > 0$ and $\mathrm{Re}\lambda_{3,4,\ldots} < 0$. Furthermore, the amplitude of the limit cycle can be approximated as

$$\hat{\rho} = \sqrt{-\frac{\mathrm{Re}\lambda_1}{\mathrm{Re}\beta_{21}}}, \tag{69}$$

while the corresponding angular frequency assumes the form

$$\omega = \mathrm{Im}\lambda_1 - \frac{\mathrm{Im}\beta_{21}}{\mathrm{Re}\beta_{21}}\mathrm{Re}\lambda_1. \tag{70}$$

The limit cycle can be transformed back to the original state space; often, the first order term provides already a good estimation for the amplitude of the self-excited oscillations. Let A_i denote the amplitude of the i-th coordinate, then

$$A_i \approx 2\hat{\rho}|q_i|, \quad i = 1, 2, \ldots, n, \tag{71}$$

where q_i is the i-th coordinate of the n-dimensional vector $\mathbf{q}$ (see (10)).

However, substituting (64), (69) and (70) into (46) provides an even better approximation of the limit cycle containing also higher harmonics:

$$\begin{aligned}\mathbf{x}_t(\vartheta) = {} & \mathbf{W}_{10}(\vartheta)\hat{\rho}\mathrm{e}^{\mathrm{i}\omega t} + \mathbf{W}_{01}(\vartheta)\hat{\rho}\mathrm{e}^{-\mathrm{i}\omega t} \\ & + \frac{1}{2}\mathbf{W}_{20}(\vartheta)\hat{\rho}^2\mathrm{e}^{2\mathrm{i}\omega t} + \mathbf{W}_{11}(\vartheta)\hat{\rho}^2 \\ & + \frac{1}{2}\mathbf{W}_{02}(\vartheta)\hat{\rho}^2\mathrm{e}^{-2\mathrm{i}\omega t} + \frac{1}{6}\mathbf{W}_{30}(\vartheta)\hat{\rho}^3\mathrm{e}^{3\mathrm{i}\omega t} \\ & + \frac{1}{2}\mathbf{W}_{21}(\vartheta)\hat{\rho}^3\mathrm{e}^{\mathrm{i}\omega t} + \frac{1}{2}\mathbf{W}_{12}(\vartheta)\hat{\rho}^3\mathrm{e}^{-\mathrm{i}\omega t} \\ & + \frac{1}{6}\mathbf{W}_{03}(\vartheta)\hat{\rho}^3\mathrm{e}^{-3\mathrm{i}\omega t} + (\hat{\rho}^4).\end{aligned} \tag{72}$$

Note that because of the summation of the complex conjugate vector valued functions, the trajectory $\mathbf{x}_t(\vartheta)$ is real. Furthermore, the real coefficient $\mathbf{W}_{11}$ represents a shift in the solution, which is a well-known phenomenon caused by non-symmetric nonlinearities.

Finally, the corresponding periodic solution is the headpoint of the trajectory, that is, $\mathbf{x}_{\mathrm{per}}(t) = \mathbf{x}_t(0)$.

This allows the closed-form analytical approximation of the limit cycle calculated exactly at the parameter point of interest, which could be further away from the corresponding Hopf bifurcation point. In contrast, the classical Hopf bifurcation calculation [29,30,65] extrapolates the dynamics from the linear stability boundary. One may also calculate the SSM up to higher orders; in the case of $\mathcal{O}(5)$ approximation, the reduced dynamics contains the second resonant term $z^3\bar{z}^2$. This yields a second degree polynomial for $\hat{\rho}$ and an even better approximation of the limit cycle (and the SSM itself) as it is demonstrated in Sect. 5.2.

The only drawback of the SSM-based approach is that the dominant eigenvalues with non-zero real part cannot be expressed in closed algebraic form for arbitrary bifurcation parameters in a delayed system. Still, there are well-developed numerical methods for the approximation of the spectrum of DDEs [32,61–64].

5 Case study

As it was also selected for a case study in [66], let us consider the simplest scalar nonlinear DDE

$$\dot{x} = -x(t-\tau) + x^3(t), \tag{73}$$

where $x \in \mathbb{R}$. Compared to the general DDE (1), in this case, the coefficients of the delay-free and delayed terms are

$$\mathbf{L} = [\,0\,] \quad \text{and} \quad \mathbf{R} = [\,-1\,], \tag{74}$$

respectively, while the nonlinearity assumes the form

$$\mathbf{N}(x(t)) = \left[\, x^3(t) \,\right]. \tag{75}$$

Note that although this is a scalar case, the variables are still in bold to make the calculation comparable to the general theoretical description of Sect. 4, while square brackets refer to 1-by-1 matrices, that is, to scalars.

The corresponding (scalar) characteristic matrix assumes the form

$$\Delta(\lambda) = \left[\, \lambda + \mathrm{e}^{-\lambda\tau} \,\right], \tag{76}$$

yielding the characteristic equation

$$\lambda + \mathrm{e}^{-\lambda\tau} = 0. \tag{77}$$

The linearized system is exponentially stable, that is, all the eigenvalues have negative real parts, if the delay τ is smaller than the critical delay [30]

$$\tau_{\mathrm{cr},1} = \frac{\pi}{2}. \tag{78}$$

Assume that λ_1 is the dominant eigenvalue of the system, which may be either real or complex. Note that in the latter case, λ_1 forms a complex conjugate pair with the other dominant root $\lambda_2 = \bar{\lambda}_1$.

In this scalar case, any 1-by-1 vector $\mathbf{q}$ satisfies

$$\Delta(\lambda_1)\mathbf{q} = [\,0\,], \text{ when } \det(\Delta(\lambda_1)) = 0; \tag{79}$$

thus, one can choose

$$\mathbf{q} = [\,1\,]. \tag{80}$$

Similarly, any scalar $\mathbf{p}$ satisfies

$$\mathbf{p}\Delta(\lambda_1) = [\,0\,], \text{ when } \det(\Delta(\lambda_1)) = 0. \tag{81}$$

The actual value of $\mathbf{p}$ can be obtained from the normalization criterion (19), which now assumes

$$\mathbf{p}(1 - \tau\mathrm{e}^{-\lambda_1\tau})\mathbf{q} = 1. \tag{82}$$

Utilizing $\Delta(\lambda_1) = [\,0\,]$, the normalization yields

$$\mathbf{p} = \left[\, \frac{1}{1+\lambda_1\tau} \,\right]. \tag{83}$$

Therefore, the eigenfunctions of $\mathcal{A}^{\odot\star}$ and $\mathcal{A}^{\odot}$ assume the forms

$$\mathbf{s}(\vartheta) = \left[\, \mathrm{e}^{\lambda_1\vartheta} \,\right], \quad \vartheta \in [-\tau, 0], \tag{84}$$

$$\mathbf{n}(\sigma) = \mathbf{p}\left(1 - (\mathrm{e}^{\lambda_1\sigma} - 1)\frac{\mathrm{e}^{-\lambda_1\tau}}{\lambda_1}\right), \quad \sigma \in [0, \tau], \tag{85}$$

respectively, considering the continuous extension at $\lambda_1 = 0$. Note that, compared to (16), $\mathbf{n}(\sigma)$ is not presented for $\sigma < 0$ and $\sigma > \tau$, since the derivative property at the boundaries will not be needed during the calculations. Utilizing the characteristic equation (77), formula (85) simplifies to

$$\mathbf{n}(\sigma) = \mathbf{p}\mathrm{e}^{\lambda_1\sigma}. \tag{86}$$

The symmetry in the nonlinearity yields

$$\mathbf{B}(\Phi, \Lambda) = \begin{cases} [\,0\,], & \text{if } \vartheta \in [-\tau, 0), \\ [\,0\,], & \text{if } \vartheta = 0, \end{cases} \tag{87}$$

$$\mathbf{C}(\Phi, \Lambda, \Gamma) = \begin{cases} [\,0\,], & \text{if } \vartheta \in [-\tau, 0), \\ 6\Phi(0)\Lambda(0)\Gamma(0), & \text{if } \vartheta = 0. \end{cases} \tag{88}$$

The following two subsections present the derivation of the SSM and the corresponding dynamics for a real dominant eigenvalue and for a dominant pair of complex conjugate eigenvalues.

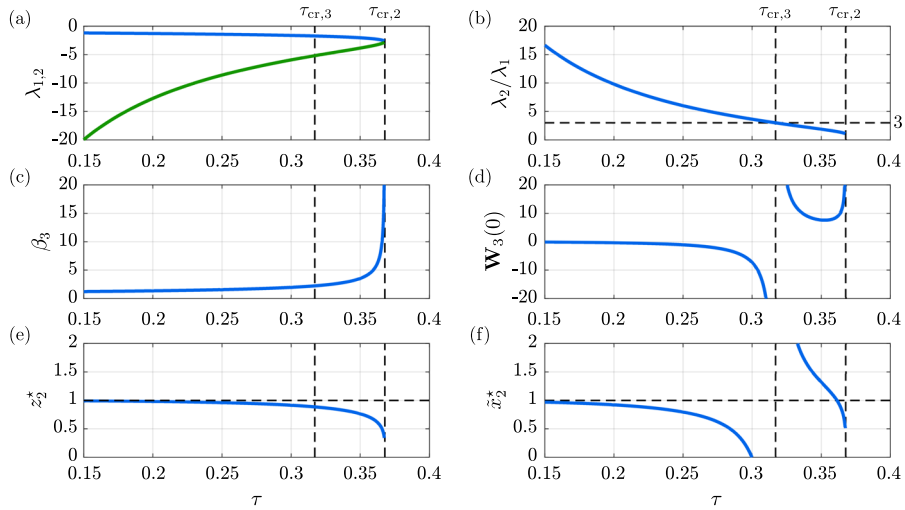

Fig. 3 Dependence of different variables on the delay τ corresponding to Example (73). Panels **a** and **b** present the evolution of the dominant characteristic roots and their ratio, respectively. Panel **c** shows the change of the coefficient of the cubic term in the reduced dynamics, while **d** visualizes the coefficient of the cubic term of the submanifold itself evaluated at $\vartheta = 0$. Finally, panels **e** and **f** refer to the non-trivial equilibrium point of the reduced order dynamics and the corresponding equilibrium transformed back to the original coordinate, respectively

5.1 The case of a dominant real eigenvalue

Let us assume that λ_1 is the real dominant eigenvalue of system (73). After carrying out the spectral submanifold calculation detailed in Sect. 4.1, the coefficients of the SSM are

$$\mathbf{W}_1(\vartheta) = \left[\, \mathrm{e}^{\lambda_1 \vartheta} \,\right], \tag{89}$$

$$\mathbf{W}_2(\vartheta) \equiv [\,0\,], \tag{90}$$

$$\begin{aligned}\mathbf{W}_3(\vartheta) &= \Delta^{-1}(3\lambda_1) 6\mathbf{s}^3(0)\mathrm{e}^{3\lambda_1\vartheta} - 3\frac{\beta_3}{\lambda_1}\mathbf{s}(\vartheta) \\ &= \left[\, \frac{6\mathrm{e}^{3\lambda_1\vartheta}}{3\lambda_1 + \mathrm{e}^{-3\lambda_1\tau}} - \frac{3\mathrm{e}^{\lambda_1\vartheta}}{\lambda_1 + \lambda_1^2\tau} \,\right],\end{aligned} \tag{91}$$

while

$$\beta_2 \equiv 0, \quad \text{and} \quad \beta_3 = \frac{1}{6}\mathbf{p}6\mathbf{s}^3(0) = \frac{1}{1+\lambda_1\tau}, \tag{92}$$

where we utilized (84) which implies that $\mathbf{s}(0) = [1]$. Here, the coefficients $\mathbf{W}_2$ and β_2 are zero, since the governing Eq. (73) lacks the second-order nonlinearity.

Figure 3 presents the two most dominant characteristic roots $\lambda_{1,2}$, their ratio, and the relevant parameters of the spectral submanifold as a function of the delay parameter τ. In the given range, both λ_1 and λ_2 are real and they are well separated for $\tau < 0.3$.

Note that in this simple system, the maximal number of real characteristic roots is 2. This can be obtained solving the characteristic Eq. (76) for $\lambda \in \mathbb{R}$, which leads to the intersections of an exponential and a linear function. These curves intersect at most twice providing the two real roots; all the other infinitely many eigenvalues are complex. Thus, in this case, the non-resonance conditions (39) have to be checked only between the two real eigenvalues.

A $\lambda_2 = 3\lambda_1$ resonance occurs when

$$\tau = \tau_{\mathrm{cr},3} := \frac{\ln 3}{2\sqrt{3}}, \tag{93}$$

$$\lambda_1 = -\sqrt{3}, \quad \text{and} \quad \lambda_2 = -3\sqrt{3}. \tag{94}$$

At this point, the $\mathbf{W}_3$ coefficient of the SSM is singular, which can also be obtained from the expression (91).

As the delay is increased the two real roots are approaching each other, they coincide at the critical value $\tau_{\mathrm{cr},2}$, above which the dominant roots form a complex conjugate pair. At this critical delay, λ_1 is the solution of the characteristic equation with multiplicity two. This means that λ_1 is not only a root of (76), but also a root of its derivative with respect to λ:

$$\frac{\partial \det(\Delta(\lambda))}{\partial \lambda} = 1 - \tau \mathrm{e}^{-\lambda\tau}. \tag{95}$$

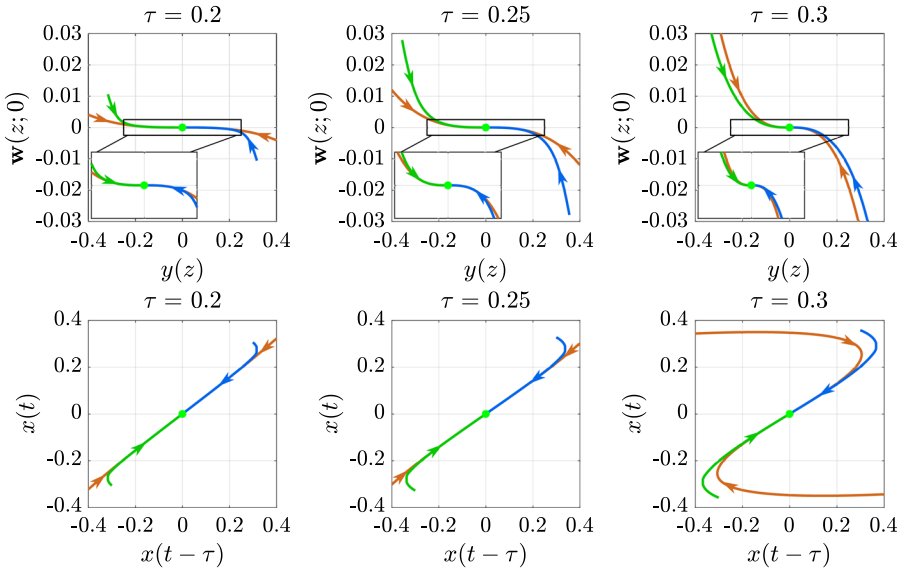

Fig. 4 Convergence of two particular trajectories towards the spectral submanifold corresponding to the dominant real root for different values of the delay τ. The brown curve indicates SSM, while the green and blue curves represent trajectories initiated from $x(t) = -0.2 - t$ and from $x(t) = 0.2 + t$ $(t \in [-\tau, 0])$, respectively

After some calculation, one obtains that

$$\tau_{\mathrm{cr},2} = \frac{1}{\mathrm{e}}, \tag{96}$$

at which

$$\lambda_{1,2} = -\mathrm{e}. \tag{97}$$

At this critical delay, both $\mathbf{W}_3$ and β_3 tend to infinity, which can be obtained from their expressions (91) and (92). Note that if a linear reduced dynamics had been assumed with $\beta_3 = 0$, then the coefficient $\mathbf{W}_3$ would remain finite. This corresponds to the SSM theory for ordinary differential equations, according to which the 1:1 resonance is allowed [11].

Substituting (89)–(91) into (29) results the current third-order approximation of the SSM:

$$\mathbf{W}(z;\vartheta) = \left[\mathrm{e}^{\lambda_1\vartheta}z + \left(\frac{\mathrm{e}^{3\lambda_1\vartheta}}{3\lambda_1 + \mathrm{e}^{-3\lambda_1\tau}} - \frac{\mathrm{e}^{\lambda_1\vartheta}}{2(\lambda_1 + \lambda_1^2\tau)}\right)z^3\right], \tag{98}$$

while the reduced dynamics is governed by the normal form of a pitchfork bifurcation:

$$\dot{z} = \lambda_1 z + \frac{1}{1+\lambda_1\tau}z^3. \tag{99}$$

Thus, beside the trivial equilibrium $z_1 = 0$, the reduced dynamics has two further equilibria at:

$$z^\star_{2,3} = \pm\sqrt{-\lambda_1(1+\lambda_1\tau)}, \tag{100}$$

see Fig. 3e where $z_2^\star$ is plotted as a function of τ.

Transforming these equilibria to the original coordinate system with the help of (98), and utilizing the characteristic Eq. (77), one obtains

$$\tilde{x}^\star_{2,3} = \pm\frac{7 - 3\lambda_1^2 + 2\ln(-\lambda_1)}{6 - 2\lambda_1^2}\sqrt{-(\lambda_1 - \lambda_1\ln(-\lambda_1))}, \tag{101}$$

see Fig. 3f depicting $\tilde{x}_2^\star$ as a function of τ. Note that in this case the real dominant eigenvalue $\lambda_1 < 0$, that is, the natural logarithm is defined for $\ln(-\lambda_1)$. In addition, the nontrivial equilibria can be obtained from the original Eq. (73), leading to the exact solutions $x^\star_{2,3} = \pm 1$. Figure 3f shows that the location of the nontrivial equilibrium estimated through (100) is not accurate enough for $\tau > 0.3$ due to the nearby resonance.

The nonlinear part of the SSM and the transformed trajectories initiated from two different initial conditions are presented in the first row of Fig. 4 for various values of the delay τ (see the details of the trajectory transformation in Appendix D). In all cases, the trajectories approach the manifold and tend to the origin along that. However, the trajectories run longer along the manifold when the time delay is small, that is, when the dominant characteristic root is increasingly

separated from the other characteristic roots of the system. Furthermore, the second row of Fig. 4 presents the same trajectories in the plane of the delayed coordinate $x(t-\tau)$ and of the current coordinate $x(t)$, which correspond to the $\mathbf{W}(z;-\tau)$ and $\mathbf{W}(z;0)$ states of the SSM, respectively. Again, the trajectories approach the manifold and tend to the origin along that.

5.2 Projection to the manifold corresponding to a pair of complex conjugate eigenvalues

As it was determined in the previous subsection, if the delay satisfies $\tau_{\mathrm{cr},2} < \tau < \tau_{\mathrm{cr},1}$, then the dominant eigenvalues of (73) form a complex conjugate pair. Let λ_1 and $\lambda_2 = \overline{\lambda}_1$ denote this dominant pair of roots.

In this case, the spectral submanifold calculation–detailed in Sect. 4.2–yields

$$\mathbf{W}_{10}(\vartheta) = \left[\, \mathrm{e}^{\lambda_1\vartheta} \,\right], \tag{102}$$

$$\mathbf{W}_{30}(\vartheta) = \Delta^{-1}(3\lambda_1)6\mathbf{s}^3(0)\mathrm{e}^{3\lambda\vartheta} = \left[\, \frac{6\mathrm{e}^{3\lambda_1\vartheta}}{3\lambda_1 + \mathrm{e}^{-3\lambda_1\tau}} \,\right], \tag{103}$$

while

$$\beta_{21} = \frac{1}{2}\mathbf{p}6\mathbf{s}^2(0)\bar{\mathbf{s}}(0) = \frac{3}{1+\lambda_1\tau}, \tag{104}$$

and so

$$\mathbf{W}_{21}(\vartheta) = \mathrm{e}^{(2\lambda_1+\overline{\lambda}_1)\vartheta}\Delta^{-1}(2\lambda_1+\overline{\lambda}_1)6\mathbf{s}^2(0)\bar{\mathbf{s}}(0) - \frac{2\beta_{21}}{\lambda_1+\overline{\lambda}_1}\mathbf{q}\mathrm{e}^{\lambda_1\vartheta} = \left[\, \frac{6\mathrm{e}^{(2\lambda_1+\overline{\lambda}_1)\vartheta}}{2\lambda_1+\overline{\lambda}_1+\mathrm{e}^{-(2\lambda_1+\overline{\lambda}_1)\tau}} - \frac{6\mathrm{e}^{\lambda_1\vartheta}}{(\lambda_1+\overline{\lambda}_1)(1+\lambda_1\tau)} \,\right]. \tag{105}$$

In the above derivations, we utilized (84), which implies that $\mathbf{s}(0) = \bar{\mathbf{s}}(0) = [1]$. Furthermore,

$$\mathbf{W}_{01} = \overline{\mathbf{W}}_{10}, \quad \mathbf{W}_{03} = \overline{\mathbf{W}}_{30}, \quad \mathbf{W}_{12} = \overline{\mathbf{W}}_{21}, \tag{106}$$

and again, the second-order terms are zero:

$$\mathbf{W}_{20} = \mathbf{W}_{11} = \mathbf{W}_{02} = [\,0\,]. \tag{107}$$

Thus, the SSM assumes the form

$$\begin{aligned}\mathbf{W}(z,\bar{z};\vartheta) = {} & \mathrm{e}^{\lambda_1\vartheta}z + \mathrm{e}^{\overline{\lambda}_1\vartheta}\bar{z} + \frac{6\mathrm{e}^{3\lambda_1\vartheta}}{3\lambda_1+\mathrm{e}^{-3\lambda_1\tau}}z^3 \\ & + \left(\frac{6\mathrm{e}^{(2\lambda_1+\overline{\lambda}_1)\vartheta}}{2\lambda_1+\overline{\lambda}_1+\mathrm{e}^{-(2\lambda_1+\overline{\lambda}_1)\tau}} - \frac{6\mathrm{e}^{\lambda_1\vartheta}}{(\lambda_1+\overline{\lambda}_1)(1+\lambda_1\tau)}\right)z^2\bar{z} \\ & + \left(\frac{6\mathrm{e}^{(2\overline{\lambda}_1+\lambda_1)\vartheta}}{2\overline{\lambda}_1+\lambda_1+\mathrm{e}^{-(2\overline{\lambda}_1+\lambda_1)\tau}} - \frac{6\mathrm{e}^{\overline{\lambda}_1\vartheta}}{(\lambda_1+\overline{\lambda}_1)(1+\overline{\lambda}_1\tau)}\right)z\bar{z}^2 \\ & + \frac{6\mathrm{e}^{3\overline{\lambda}_1\vartheta}}{3\overline{\lambda}_1+\mathrm{e}^{-3\overline{\lambda}_1\tau}}\bar{z}^3 + \mathcal{O}(|z|^5),\end{aligned} \tag{108}$$

while the corresponding reduced dynamics is governed by the normal form

$$\dot{z} = \lambda_1 z + \frac{3}{1+\lambda_1\tau}z^2\bar{z} + \mathcal{O}(|z|^5). \tag{109}$$

As it was stated in (68), a limit cycle exists if $\mathrm{Re}\lambda_1/\mathrm{Re}\beta_{21} < 0$. According to (69), (70), the amplitude and the angular frequency of this limit cycle assume the forms

$$\hat{\rho} = \sqrt{-\frac{\mathrm{Re}\lambda_1}{\mathrm{Re}\left(\frac{3}{1+\lambda_1\tau}\right)}}, \tag{110}$$

$$\omega = \mathrm{Im}\lambda_1\left(1 + \frac{\tau\mathrm{Re}\lambda_1}{1+\tau\mathrm{Re}\lambda_1}\right), \tag{111}$$

respectively.

Evaluating $\mathbf{W}(z,\bar{z};\vartheta)$ at $z = \hat{\rho}\mathrm{e}^{\mathrm{i}\omega t}$ and considering $\vartheta = 0$ yield the formula of the limit cycle in the original coordinate (see also (72)):

$$\begin{aligned}x_{\mathrm{per}}(t) = {} & \hat{\rho}\left(\mathrm{e}^{\mathrm{i}\omega t} + \mathrm{e}^{-\mathrm{i}\omega t}\right) \\ & + \hat{\rho}^3\left(\frac{2\mathrm{e}^{\mathrm{i}\omega t}}{2\lambda_1+\overline{\lambda}_1+\mathrm{e}^{-(2\lambda_1+\overline{\lambda}_1)\tau}} - \frac{2\mathrm{e}^{\mathrm{i}\omega t}}{(\lambda_1+\overline{\lambda}_1)(1+\lambda_1\tau)}\right. \\ & + \frac{2\mathrm{e}^{-\mathrm{i}\omega t}}{2\overline{\lambda}_1+\lambda_1+\mathrm{e}^{-(2\overline{\lambda}_1+\lambda_1)\tau}} - \frac{2\mathrm{e}^{-\mathrm{i}\omega t}}{(\lambda_1+\overline{\lambda}_1)(1+\overline{\lambda}_1\tau)} \\ & \left. + \frac{\mathrm{e}^{3\mathrm{i}\omega t}}{3\lambda_1+\mathrm{e}^{-3\lambda_1\tau}} + \frac{\mathrm{e}^{-3\mathrm{i}\omega t}}{3\overline{\lambda}_1+\mathrm{e}^{-3\overline{\lambda}_1\tau}}\right) + \mathcal{O}\left(\hat{\rho}^5\right),\end{aligned} \tag{112}$$

where $\hat{\rho}$ and ω are given by (110) and (111), respectively. That is, the SSM algorithm results a closed-form analytic approximation of the limit cycle exactly at the parameter point of interest. Moreover, the expression contains not only the first Fourier term of the self-excited oscillation but also the higher harmonics.

The first row of Fig. 5 present the SSM and the transformed trajectories above the space spanned by

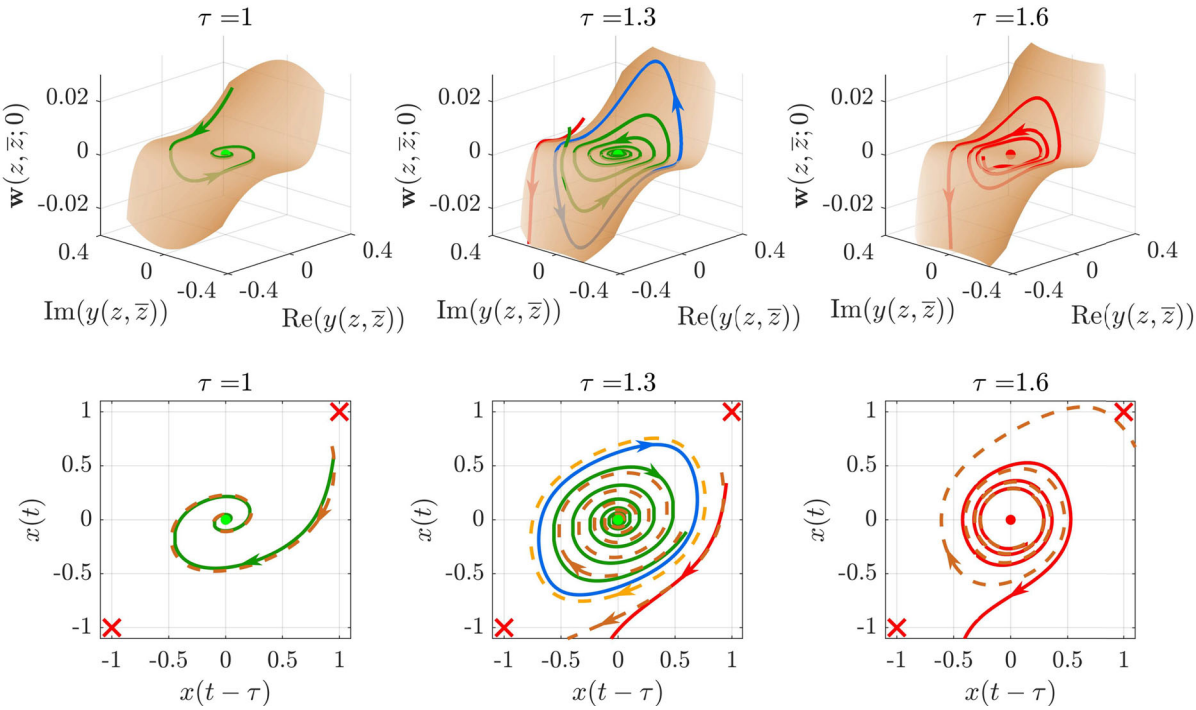

Fig. 5 Convergence of trajectories towards the spectral submanifold corresponding to the dominant pair of complex conjugate roots for various values of the delay τ. The brown surface refers to the spectral submanifold, while the green and red curves represent converging and diverging trajectories, respectively. Finally, the blue closed curve is an unstable limit cycle determined with DDE-BIFTOOL. In the panels of the second row, the brown dashed curves are trajectories initiated on the SSM and obtained with the reduced dynamics, while the orange dashed curve is the approximation of the limit cycle based on the reduced order model. The initial conditions of the trajectories are summarized in Table 1. The trivial equilibrium is indicated with green or red dot depending on whether it is stable or unstable, while red crosses refer to the unstable nontrivial fixed points

Table 1 Initial conditions of the trajectories visualized in Fig. 5. The functions are defined in the interval $t \in [-\tau, 0]$

	Convergent traj.	Divergent traj.
$\tau = 1$	$x(t) = 0.95$	–
$\tau = 1.3$	$x(t) = 0.6$	$x(t) = 0.95$
$\tau = 1.6$	–	$x(t) = 0.15 - 0.1t$

the real and imaginary parts of the eigenfunction **s** for various delay values. The brown surface refers to the spectral submanifold, while the green and red curves represent converging and diverging trajectories, respectively. Finally, the blue closed curve is a limit cycle determined with DDE-BIFTOOL [61,67]. Observe that all trajectories are running close to the SSM. Selecting the initial condition $x(t) \equiv 0.95$ ($t \in [-\tau, 0]$), the trajectory converges to the origin for $\tau = 1$ while it diverges for $\tau = 1.3$ (see also Table 1). The latter occurs due to the presence of the unstable limit cycle. In case of $\tau = 1.6$, the origin is unstable since $\tau > \tau_{\mathrm{cr},1}$; still, the trajectory tends to the SSM and remains close to that while it is spiraling outward.

The second row of Fig. 5 presents the same trajectories in the plane of the actual and the delayed states. The brown dashed curves represent trajectories on the SSM calculated based on the reduced dynamics (109). The initial conditions for the SSM-based trajectories were generated by projecting the initial condition of the reference trajectory to the SSM; this explains the phase shift. Still, the SSM-based trajectories approximate well the reference trajectories. Moreover, the orange dashed curve refers to the limit cycle calculated from the 3rd order SSM, which is also in good agreement with the one obtained by DDE-BIFTOOL.

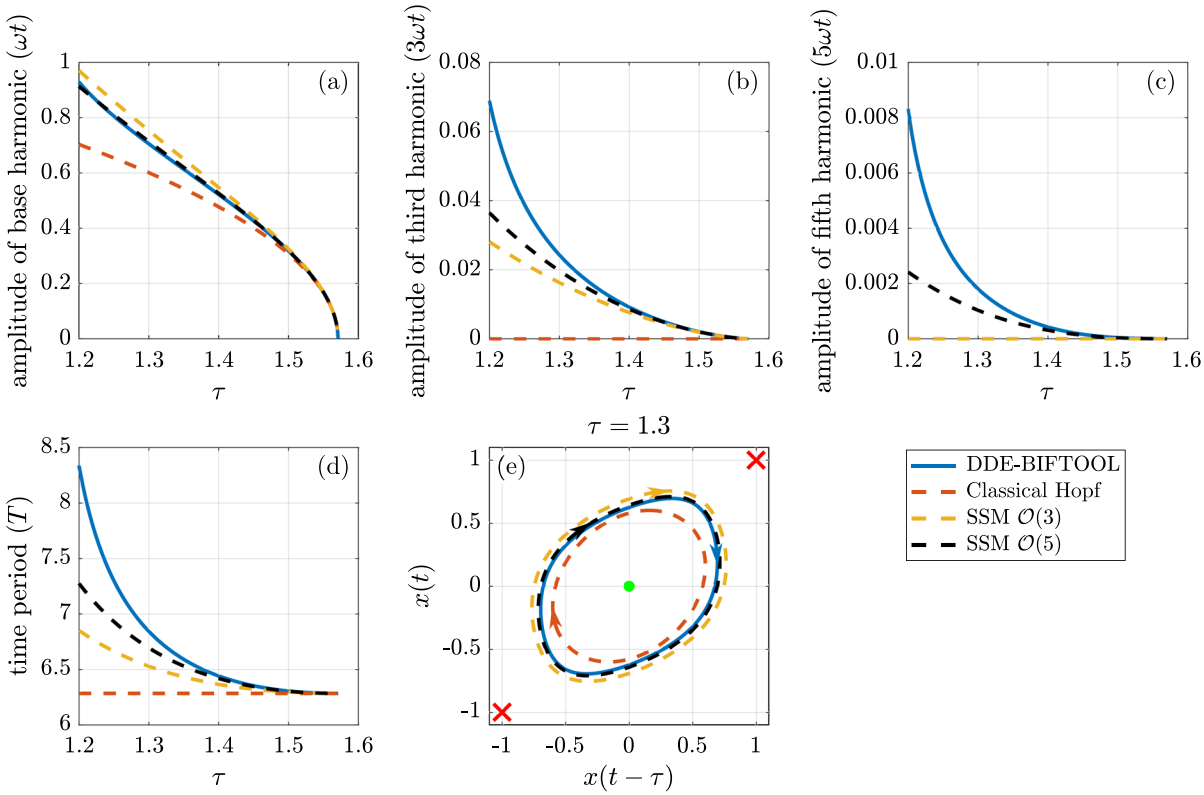

Fig. 6 Comparison of the limit cycle obtained with DDE-BIFTOOL, with the traditional Hopf bifurcation calculation and with spectral submanifolds of order 3 and 5. Panels **a**–**c** present the different harmonics of the limit cycle, panel **d** shows the corresponding time period, while panel **e** shows the limit cycles in the plane of the delayed and actual states for $\tau = 1.3$

Figure 6 presents the evolution of the unstable limit cycle as the bifurcation parameter τ is varied. Fast Fourier transform was applied to the limit cycle: panel (a) presents the bifurcation diagram for the base harmonic, while panels (b) and (c) present the bifurcation diagrams for the higher harmonics. The blue curve serves as a reference, determined with DDE-BIFTOOL, the dashed red line is the result of the classical Hopf bifurcation calculation [30], while the dashed orange and black lines present the 3rd and 5th order SSM-based approximations. By classical Hopf, we mean the calculation of the Poincaré-Lyapunov coefficient and the root tendency at the Hopf bifurcation boundary, and then the extrapolation of the limit cycle further away from the bifurcation point at $\tau_{\mathrm{cr},1}$. During this extrapolation, the time period of oscillation is assumed to be constant, while the limit cycle contains only the base harmonic. As it can be observed, the higher-order SSM-based approximation not only introduces higher harmonics, but it also effects the base harmonic yielding excellent match with the reference.

Panel (d) presents the time period of the limit cycle as the delay varies. Again, the SSM-based approximation is better than assuming constant time period, and it improves further when the SSM is calculated up to higher order. Finally, panel (e) visualises the limit cycle at $\tau = 1.3$ and it shows that the 5th order SSM approximation indeed provides an excellent match with the reference given by DDE-BIFTOOL.

6 Conclusion

In the present paper, we extended the powerful concept of spectral submanifolds to time delay systems. Spectral projections were carried out to an SSM corresponding to a real dominant eigenvalue and to an SSM corresponding to a pair of complex conjugate eigenvalues.

These results can be generalized also to large dimensional spectral subspaces, however, the corresponding derivations may become lengthy.

In the case of complex conjugate dominant eigenvalues, the method allowed an improved approximation of self-excited oscillations exactly at the parameter point of interest, which could be further away from the corresponding Hopf bifurcation point. In contrast, the classical Hopf bifurcation calculation extrapolates the limit cycle while using the parameters from the linear stability boundary.

The theoretical derivation was followed by a case study, which demonstrated the effectiveness of the method. A nonlinear scalar DDE was investigated analytically, which presented the accuracy of the algorithm together with its limitations at parameter combinations close to resonances. Furthermore, it also demonstrated how precisely a limit cycle can be approximated.

Note that the investigation of the existence and uniqueness of the delayed SSMs is a part of future research. Nevertheless, the results show a good agreement with the simulations, and we consider that the algorithm can be useful from an engineering point of view similarly to the SSMs applied for finite element and finite volume models of partial differential Eqs. [18,20,22]. In those cases the SSM can be proven to be unique and exist for the ODE corresponding to the approximate discretized model, however, it is an open question whether the SSM of the original partial differential equation exists.

Finally, as a future direction, we plan to extend the SSM to calculations for periodically forced time delay systems.

Acknowledgements The Authors are thankful to Tamás Molnár for discussions on the mathematical background of the sun-star calculus.

Funding Open access funding provided by Budapest University of Technology and Economics. The research reported in this paper has been supported by the Hungarian National Research, Development and Innovation Office (NKFI-KKP-133846). Gábor Orosz acknowledges the support of Hungarian Academy of Sciences within the Distinguished Guest Fellowship Programme during 2022 and the support of the Fulbright Foundation during the award period 2023-2024.

Data availability Data sharing is not applicable to this article as no datasets were generated or analysed during the current study.

Code availability The MATLAB codes for the calculation of the SSM in time delay systems are available at https://github.com/benceszaksz/delayedSSM.

Declarations

Conflict of interest The authors declare that they have no Conflict of interest.

Appendix A Eigenfunctions of the operators

Let us assume that the linearized dynamics is governed by the Stieltjes type DDE:

$$\dot{\mathbf{x}}_t = \int_0^\tau \mathrm{d}\xi(\theta)\mathbf{x}_t(-\theta), \tag{A1}$$

where

$$\xi(\theta) = \mathbf{L}\hat{H}(\theta) + \mathbf{R}H(\theta-\tau), \tag{A2}$$

with

$$H(\theta) = \begin{cases} 1, & \text{if } \theta \geq 0, \\ 0, & \text{if } \theta < 0, \end{cases} \tag{A3}$$

and

$$\hat{H}(\theta) = \begin{cases} 1, & \text{if } \theta > 0, \\ 0, & \text{if } \theta \leq 0. \end{cases} \tag{A4}$$

Fig. 7a–c present these heaviside step functions and the function of bounded variation $\xi(\theta)$ to visualize the nature of their discontinuities.

Then, the corresponding linear operators assume the form (see [44,45]):

$$\mathcal{A}^{\odot\star}\Phi = \begin{cases} \frac{\mathrm{d}\Phi}{\mathrm{d}\vartheta}(\vartheta), & \text{if } \vartheta \in [-\tau, 0), \\ \int_0^\tau \mathrm{d}\xi(\theta)\Phi(-\theta), & \text{if } \vartheta = 0, \end{cases} \tag{A5}$$

and

$$\mathcal{A}^{\odot}\Psi = \frac{\mathrm{d}\Psi}{\mathrm{d}\sigma}(\sigma) + \Psi(0)\int_0^\sigma \mathrm{d}\xi(\varphi), \text{ if } \sigma \in [0,\tau]. \tag{A6}$$

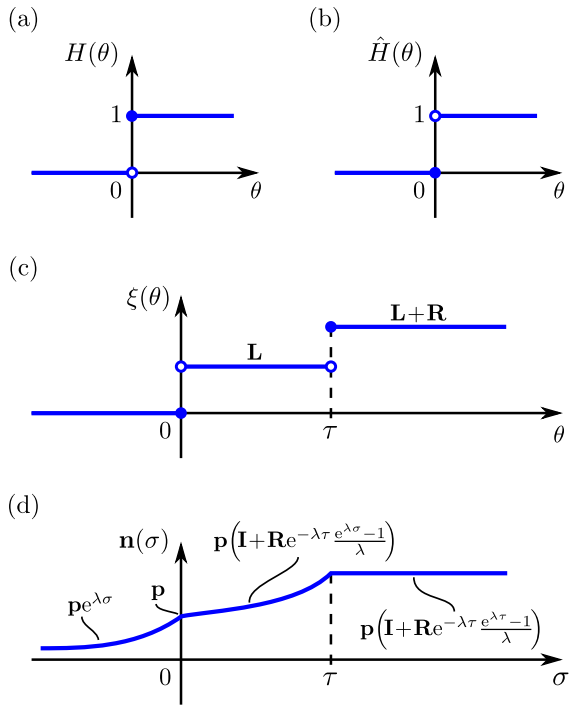

Fig. 7 Panels **a** and **b** visualize the heaviside step functions $H(\theta)$ and $\hat{H}(\theta)$, respectively, panel **c** refers to the function $\xi(\theta)$ that determines the dynamics, while panel **d** illustrates the eigenfunction $\mathbf{n}(\sigma)$ of the operator $\mathcal{A}^{\odot}$

Furthermore, the characteristic matrix and its derivative take the form

$$\Delta(\lambda) = \lambda\mathbf{I} - \int_0^\tau \mathrm{e}^{-\lambda\theta}\mathrm{d}\xi(\theta), \tag{A7}$$

and

$$\Delta'(\lambda) = \mathbf{I} - \int_0^\tau -\theta\mathrm{e}^{-\lambda\theta}\mathrm{d}\xi(\theta). \tag{A8}$$

Appendix A.1 Domain restriction of operator $\mathcal{A}^{\odot}$

The adjoint operator is defined through (14), and this is the source of the restriction of the corresponding domain as well. Let us derive the left- and right-hand side in more detail.

According to the definition of the pairing, the right-hand side of (14) assumes the form

$$\langle\Psi, \mathcal{A}^{\odot\star}\Phi\rangle = \Psi(0)(\mathcal{A}^{\odot\star}\Phi)(0) + \int_0^\tau \frac{\mathrm{d}\Psi}{\mathrm{d}\theta}(\theta)(\mathcal{A}^{\odot\star}\Phi)(-\theta)\mathrm{d}\theta. \tag{A9}$$

Then, utilizing the definition (A5), one obtains

$$\langle\Psi, \mathcal{A}^{\odot\star}\Phi\rangle = \Psi(0)\int_0^\tau \mathrm{d}\xi(\theta)\Phi(-\theta) + \int_0^\tau \frac{\mathrm{d}\Psi}{\mathrm{d}\theta}(\theta)\frac{\mathrm{d}\Phi}{\mathrm{d}\theta}(-\theta)\mathrm{d}\theta. \tag{A10}$$

Similarly, the left-hand side of (14) takes the form

$$\langle\mathcal{A}^{\odot}\Psi, \Phi\rangle = (\mathcal{A}^{\odot}\Psi)(0)\Phi(0) + \int_0^\tau \frac{\mathrm{d}(\mathcal{A}^{\odot}\Psi)}{\mathrm{d}\theta}(\theta)\Phi(-\theta)\mathrm{d}\theta, \tag{A11}$$

which can be reformulated with the help of (A6) as

$$\langle\mathcal{A}^{\odot}\Psi, \Phi\rangle = (\mathcal{A}^{\odot}\Psi)(0)\Phi(0) + \int_0^\tau \frac{\mathrm{d}^2\Psi}{\mathrm{d}\theta^2}(\theta)\Phi(-\theta)\mathrm{d}\theta + \Psi(0)\int_0^\tau \frac{\mathrm{d}}{\mathrm{d}\theta}\int_0^\theta \mathrm{d}\xi(\varphi)\Phi(-\theta)\mathrm{d}\theta. \tag{A12}$$

Finally, the partial integration of the second term and the simplification of the third term yields

$$\langle\mathcal{A}^{\odot}\Psi, \Phi\rangle = (\mathcal{A}^{\odot}\Psi)(0)\Phi(0) + \frac{\mathrm{d}\Psi}{\mathrm{d}\theta}(\tau)\Phi(-\tau) - \frac{\mathrm{d}\Psi}{\mathrm{d}\theta}(0)\Phi(0) + \int_0^\tau \frac{\mathrm{d}\Psi}{\mathrm{d}\theta}(\theta)\frac{\mathrm{d}\Phi}{\mathrm{d}\theta}(-\theta)\mathrm{d}\theta + \Psi(0)\int_0^\tau \mathrm{d}\xi(\theta)\Phi(-\theta). \tag{A13}$$

Then, since

$$(\mathcal{A}^{\odot}\Psi)(0) = \frac{\mathrm{d}\Psi}{\mathrm{d}\theta}(0), \tag{A14}$$

the expressions (A10) and (A13) are equal if

$$\frac{\mathrm{d}\Psi}{\mathrm{d}\theta}(\tau) = \mathbf{0}. \tag{A15}$$

This domain restriction is presented in (12).

Appendix A.2 Eigenfunction of operator $\mathcal{A}^{\odot\star}$

The eigenfunction $\mathbf{s}(\vartheta)$ corresponding to the eigenvalue λ of $\mathcal{A}^{\odot\star}$ satisfies (8) yielding the boundary value problem:

$$\frac{\mathrm{d}\mathbf{s}}{\mathrm{d}\vartheta}(\vartheta) = \lambda\mathbf{s}(\vartheta), \text{ if } \vartheta \in [-\tau, 0), \tag{A16}$$

with the boundary condition

$$\int_0^\tau \mathrm{d}\xi(\theta)\mathbf{s}(-\theta) = \lambda\mathbf{s}(0), \tag{A17}$$

at $\vartheta = 0$. The solution yields the eigenfunction

$$\mathbf{s}(\vartheta) = \mathbf{q}\mathrm{e}^{-\lambda\tau}, \tag{A18}$$

where the vector $\mathbf{q}$ satisfies $\Delta(\lambda)\mathbf{q} = \mathbf{0}$.

Appendix A.3 Eigenfunction of operator $\mathcal{A}^{\odot}$

Similarly, the eigenfunction $\mathbf{n}(\sigma)$ of the adjoint operator $\mathcal{A}^{\odot}$ is the solution of

$$\frac{\mathrm{d}\mathbf{n}}{\mathrm{d}\sigma}(\sigma) + \mathbf{n}(0)\int_0^\sigma \mathrm{d}\xi(\varphi) = \lambda\mathbf{n}(\sigma). \tag{A19}$$

Utilizing the variation of constants formula yields

$$\mathbf{n}(\sigma) = \mathrm{e}^{\lambda\sigma}\mathbf{n}(0) - \int_0^\sigma \mathrm{e}^{\lambda(\sigma-\theta)}\mathbf{n}(0)\int_0^\theta \mathrm{d}\xi(\varphi)\mathrm{d}\theta, \tag{A20}$$

where $\mathbf{n}(0) = \mathbf{p}$, such that $\mathbf{p}\Delta(\lambda) = \mathbf{0}$. Thus, the eigenfunction assumes

$$\mathbf{n}(\sigma) = \mathrm{e}^{\lambda\sigma}\mathbf{p}\left(\mathbf{I} - \int_0^\sigma \mathrm{e}^{-\lambda\theta}\int_0^\theta \mathrm{d}\xi(\varphi)\mathrm{d}\theta\right). \tag{A21}$$

Applying partial integration yields

$$\mathbf{n}(\sigma) = \mathrm{e}^{\lambda\sigma}\mathbf{p}\left(\mathbf{I} + \frac{\mathrm{e}^{-\lambda\sigma}}{\lambda}\int_0^\sigma \mathrm{d}\xi(\varphi) - \int_0^\sigma \frac{\mathrm{e}^{-\lambda\theta}}{\lambda}\mathrm{d}\xi(\theta)\right). \tag{A22}$$

Then, introducing

$$\mathbf{f}(\lambda;\sigma) = \int_0^\sigma \mathrm{e}^{-\lambda\theta}\mathrm{d}\xi(\theta), \tag{A23}$$

and utilizing that

$$\int_0^\sigma \mathrm{e}^{\lambda\theta}\frac{\mathrm{d}\mathbf{f}}{\mathrm{d}\theta}(\lambda;\theta)\mathrm{d}\theta = \int_0^\sigma \mathrm{d}\xi(\theta), \tag{A24}$$

the above expression can be rewritten as

$$\mathbf{n}(\sigma) = \mathbf{p}\left(\mathrm{e}^{\lambda\sigma}\mathbf{I} + \int_0^\sigma \frac{\mathrm{e}^{-\lambda\varphi}}{\lambda}\frac{\mathrm{d}\mathbf{f}}{\mathrm{d}\varphi}(\lambda;\varphi)\mathrm{d}\varphi - \frac{\mathrm{e}^{\lambda\sigma}}{\lambda}\mathbf{f}(\lambda;\sigma)\right). \tag{A25}$$

After this, let us carry out a second partial integration yielding

$$\begin{aligned}\mathbf{n}(\sigma) &= \mathbf{p}\left(\mathrm{e}^{\lambda\sigma}\mathbf{I} - \int_0^\sigma \mathrm{e}^{\lambda\varphi}\mathbf{f}(\lambda;\varphi)\mathrm{d}\varphi\right)\\ &= \mathbf{p}\left(\left(1 + \int_0^\sigma \lambda\mathrm{e}^{\lambda\varphi}\mathrm{d}\varphi\right)\mathbf{I} - \int_0^\sigma \mathrm{e}^{\lambda\varphi}\mathbf{f}(\lambda;\varphi)\mathrm{d}\varphi\right)\\ &= \mathbf{p}\left(\mathbf{I} + \int_0^\sigma \mathrm{e}^{\lambda\varphi}(\mathbf{f}(\lambda;\tau) - \mathbf{f}(\lambda;\varphi))\mathrm{d}\varphi\right.\\ &\quad \left. + \int_0^\sigma \mathrm{e}^{\lambda\varphi}\mathrm{d}\varphi\Delta(\lambda)\right),\end{aligned} \tag{A26}$$

where we utilized that $\lambda\mathbf{I} = \mathbf{f}(\lambda;\tau) + \Delta(\lambda)$, which is obtained from the combination of (A7) and (A23).

Finally, since $\mathbf{p}\Delta(\lambda) = \mathbf{0}$, this expression simplifies to

$$\begin{aligned}\mathbf{n}(\sigma) &= \mathbf{p}\left(\mathbf{I} + \int_0^\sigma \mathrm{e}^{\lambda\varphi}(\mathbf{f}(\lambda;\tau) - \mathbf{f}(\lambda;\varphi))\mathrm{d}\varphi\right)\\ &= \mathbf{p}\left(\mathbf{I} + \int_0^\sigma \int_\varphi^\tau \mathrm{e}^{\lambda(\varphi-\alpha)}\mathrm{d}\xi(\alpha)\mathrm{d}\varphi\right),\end{aligned} \tag{A27}$$

which was also obtained in [45].

Then, we can substitute (A2) and carry out a partial integration yielding

$$\begin{aligned}\mathbf{n}(\sigma) = \mathbf{p}\left(\mathbf{I} + \int_0^\sigma [\mathrm{e}^{\lambda(\varphi-\alpha)}(\mathbf{L}\hat{H}(\alpha) + \mathbf{R}H(\alpha-\tau))]_\varphi^\tau \mathrm{d}\varphi\right.\\ \left. - \int_0^\sigma \int_\varphi^\tau (-\lambda)\mathrm{e}^{\lambda(\varphi-\alpha)}(\mathbf{L}\hat{H}(\alpha) + \mathbf{R}H(\alpha-\tau))\mathrm{d}\alpha\mathrm{d}\varphi\right).\end{aligned} \tag{A28}$$

The result of the nested integration is

$$\mathbf{n}(\sigma) = \mathbf{p}\left(\mathbf{I} + \int_0^\sigma \Upsilon(\varphi)\mathrm{d}\varphi\right), \tag{A29}$$

with

$$\Upsilon(\varphi) = \begin{cases} \mathrm{e}^{\lambda\varphi}\mathbf{L} + \mathrm{e}^{\lambda(\varphi-\tau)}\mathbf{R}, & \varphi \le 0, \\ \mathrm{e}^{\lambda(\varphi-\tau)}\mathbf{R}, & \varphi \in (0,\tau), \\ \mathbf{0}, & \varphi \ge \tau. \end{cases} \tag{A30}$$

This leads to the expression of the eigenfunction in the form:

$$\mathbf{n}(\sigma) = \begin{cases} \mathbf{p}\left(\mathrm{I} + \frac{\mathrm{e}^{\lambda\sigma}-1}{\lambda}(\mathbf{L} + \mathbf{R}\mathrm{e}^{-\lambda\tau})\right), & \text{if } \sigma \le 0, \\ \mathbf{p}\left(\mathbf{I} + \mathbf{R}\mathrm{e}^{-\lambda\tau}\frac{\mathrm{e}^{\lambda\sigma}-1}{\lambda}\right), & \text{if } \sigma \in (0,\tau), \\ \mathbf{p}\left(\mathbf{I} + \mathbf{R}\mathrm{e}^{-\lambda\tau}\frac{\mathrm{e}^{\lambda\tau}-1}{\lambda}\right), & \text{if } \sigma \ge \tau. \end{cases} \tag{A31}$$

Finally, utilizing $\mathbf{p}\Delta(\lambda) = \mathbf{0}$, the latter expression simplifies to the form presented in (16).

Figure 7(d) presents the eigenfunction $\mathbf{n}(\sigma)$ illustrating that it is a continuous function, which is constant for $\sigma \ge \tau$. Note that the derivative property in the domain restriction (12) assumes the right derivative:

$$\frac{\mathrm{d}\mathbf{n}}{\mathrm{d}\sigma}(\tau) := \lim_{\sigma\to\tau^+}\frac{\mathrm{d}\mathbf{n}}{\mathrm{d}\sigma}(\sigma) = 0, \tag{A32}$$

which is fulfilled by the eigenfunction (A31).

Appendix B Homological equation in the case of complex dominant eigenvalues

The homological equation (48) assumes the form

$$\begin{aligned} &\lambda_1 z\mathbf{W}_{10} + \lambda_1\mathbf{W}_{20}z^2 + \lambda_1\mathbf{W}_{11}z\bar{z} + \frac{1}{2}\lambda_1\mathbf{W}_{30}z^3 \\ &+\lambda_1\mathbf{W}_{21}z^2\bar{z} + \frac{1}{2}\lambda_1\mathbf{W}_{12}z\bar{z}^2 + \beta_{21}z^2\bar{z}\mathbf{s} + \bar{\lambda}_1\bar{z}\mathbf{s} \\ &+\bar{\lambda}_1\mathbf{W}_{11}z\bar{z} + \bar{\lambda}_1\mathbf{W}_{02}\bar{z}^2 + \frac{1}{2}\bar{\lambda}_1\mathbf{W}_{21}z^2\bar{z} \\ &+\bar{\lambda}_1\mathbf{W}_{12}z\bar{z}^2 + \frac{1}{2}\bar{\lambda}_1\mathbf{W}_{03}\bar{z}^3 + \bar{\beta}_{21}z\bar{z}^2\bar{\mathbf{s}} \\ &= \mathcal{A}^{\odot\star}\mathbf{W}_{10}z + \mathcal{A}^{\odot\star}\mathbf{W}_{01}\bar{z} + \frac{1}{2}\mathcal{A}^{\odot\star}\mathbf{W}_{20}z^2 \\ &+\mathcal{A}^{\odot\star}\mathbf{W}_{11}z\bar{z} + \frac{1}{2}\mathcal{A}^{\odot\star}\mathbf{W}_{02}\bar{z}^2 + \frac{1}{6}\mathcal{A}^{\odot\star}\mathbf{W}_{30}z^3 \\ &+\frac{1}{2}\mathcal{A}^{\odot\star}\mathbf{W}_{21}z^2\bar{z} + \frac{1}{2}\mathcal{A}^{\odot\star}\mathbf{W}_{12}z\bar{z}^2 \\ &+\frac{1}{6}\mathcal{A}^{\odot\star}\mathbf{W}_{03}\bar{z}^3 + \frac{1}{2}\mathbf{B}(\mathbf{s},\mathbf{s})z^2 + \mathbf{B}(\mathbf{s},\bar{\mathbf{s}})z\bar{z} \\ &+\frac{1}{2}\mathbf{B}(\bar{\mathbf{s}},\bar{\mathbf{s}})\bar{z}^2 + \frac{1}{2}\mathbf{B}(\mathbf{s},\mathbf{W}_{20})z^3 + \mathbf{B}(\mathbf{s},\mathbf{W}_{11})z^2\bar{z} \\ &+\frac{1}{2}\mathbf{B}(\mathbf{s},\mathbf{W}_{02})z\bar{z}^2 + \frac{1}{2}\mathbf{B}(\bar{\mathbf{s}},\mathbf{W}_{20})z^2\bar{z} \\ &+\mathbf{B}(\bar{\mathbf{s}},\mathbf{W}_{11})z\bar{z}^2 + \frac{1}{2}\mathbf{B}(\bar{\mathbf{s}},\mathbf{W}_{02})\bar{z}^3 \\ &+\frac{1}{6}\mathbf{C}(\mathbf{s},\mathbf{s},\mathbf{s})z^3 + \frac{1}{2}\mathbf{C}(\bar{\mathbf{s}},\mathbf{s},\mathbf{s})z^2\bar{z} \\ &+\frac{1}{2}\mathbf{C}(\bar{\mathbf{s}},\bar{\mathbf{s}},\mathbf{s})z\bar{z}^2 + \frac{1}{6}\mathbf{C}(\bar{\mathbf{s}},\bar{\mathbf{s}},\bar{\mathbf{s}})\bar{z}^3. \end{aligned} \tag{B33}$$

Note that in the arguments of the nonlinear terms $\mathbf{B}$ and $\mathbf{C}$, it is already utilized that

$$\mathbf{W}_{10} = \mathbf{s}, \quad \text{and} \quad \mathbf{W}_{01} = \bar{\mathbf{s}}. \tag{B34}$$

Appendix C Solution of the homological equations

In the homological Eqs. (32) and (48), balancing the coefficients of the powers of z leads to (35), (37) or to (51)-(54), which all can be written in the general form:

$$(\tilde{\lambda}\mathcal{I} - \mathcal{A}^{\odot\star})\Phi(\vartheta) = \Psi(\vartheta), \tag{C35}$$

where $\tilde{\lambda}$ is the corresponding linear combination of the dominant eigenvalue(s) and $\Phi \in \mathcal{B}(\vartheta)$ is the coefficient of the SSM, which we want to obtain. Furthermore, the general form of the right-hand side is

$$\Psi(\vartheta) = \begin{cases} \Psi_1\mathrm{e}^{\hat{\lambda}\vartheta}, & \text{if } \vartheta \in [-\tau, 0), \\ \Psi_0 + \Psi_1, & \text{if } \vartheta = 0. \end{cases} \tag{C36}$$

Assume that $\tilde{\lambda}$ is not in the kernel of $\mathcal{A}^{\odot\star}$, and $\tilde{\lambda} \neq \hat{\lambda}$. Then, applying the operator $\mathcal{A}^{\odot\star}$ yields the boundary value problem

$$\tilde{\lambda}\Phi(\vartheta) - \frac{\mathrm{d}\Phi(\vartheta)}{\mathrm{d}\vartheta} = \Psi_1\mathrm{e}^{\hat{\lambda}\vartheta}, \quad \vartheta \in [-\tau, 0), \tag{C37}$$

with the boundary condition

$$\tilde{\lambda}\Phi(0) - \mathbf{L}\Phi(0) - \mathbf{R}\Phi(-\tau) = \Psi_0 + \Psi_1, \tag{C38}$$

at $\vartheta = 0$. The solution of (C37) is

$$\Phi(\vartheta) = \mathbf{t}\mathrm{e}^{\tilde{\lambda}\vartheta} + \frac{\Psi_1\mathrm{e}^{\hat{\lambda}\vartheta}}{\tilde{\lambda} - \hat{\lambda}}, \tag{C39}$$

where the coefficient vector $\mathbf{t}$ can be determined from the boundary condition (C38), which yields

$$\begin{aligned} &\tilde{\lambda}\left(\mathbf{t} + \frac{\Psi_1}{\tilde{\lambda} - \hat{\lambda}}\right) - \mathbf{L}\left(\mathbf{t} + \frac{\Psi_1}{\tilde{\lambda} - \hat{\lambda}}\right) \\ &\quad - \mathbf{R}\left(\mathbf{t}\mathrm{e}^{-\tilde{\lambda}\tau} + \frac{\Psi_1\mathrm{e}^{-\hat{\lambda}\tau}}{\tilde{\lambda} - \hat{\lambda}}\right) = \Psi_0 + \Psi_1. \end{aligned} \tag{C40}$$

Utilizing the definition of the characteristic matrix (6), the above equation takes the form

$$\Delta(\tilde{\lambda})\mathbf{t} + \Delta(\hat{\lambda})\frac{\Psi_1}{\tilde{\lambda} - \hat{\lambda}} + \Psi_1 = \Psi_0 + \Psi_1, \tag{C41}$$

from which $\mathbf{t}$ can be expressed as:

$$\mathbf{t} = \Delta^{-1}(\tilde{\lambda})\left(\Psi_0 - \Delta(\hat{\lambda})\frac{\Psi_1}{\tilde{\lambda}-\hat{\lambda}}\right). \tag{C42}$$

Thus, the solution of the boundary value problem assumes the form

$$\Phi(\vartheta) = \mathrm{e}^{\tilde{\lambda}\vartheta}\Delta^{-1}(\tilde{\lambda})\left(\Psi_0 - \Delta(\hat{\lambda})\frac{\Psi_1}{\tilde{\lambda}-\hat{\lambda}}\right) + \frac{\Psi_1 \mathrm{e}^{\hat{\lambda}\vartheta}}{\tilde{\lambda}-\hat{\lambda}}. \tag{C43}$$

Note that the inverse of the characteristic matrix implies that resonance occurs when $\tilde{\lambda}$ is an eigenvalue of the system.

This above expression simplifies under certain conditions:

- If Ψ_1 is in the nullspace of the characteristic matrix $\Delta(\hat{\lambda})$, then the solution takes the form

  $$\Phi(\vartheta) = \mathrm{e}^{\tilde{\lambda}\vartheta}\Delta^{-1}(\tilde{\lambda})\Psi_0 + \frac{\Psi_1 \mathrm{e}^{\hat{\lambda}\vartheta}}{\tilde{\lambda}-\hat{\lambda}}. \tag{C44}$$

  This occurs, when $\mathbf{W}_2(\vartheta)$, $\mathbf{W}_3(\vartheta)$ and $\mathbf{W}_{21}(\vartheta)$ are obtained. In these cases $\hat{\lambda}$ equals to the dominant eigenvalue λ, and Ψ_1 is a scalar multiple of the vector $\mathbf{q}$.
- If the right-hand side of (C35) consist only of nonlinear terms, that is $\Psi_1 = \mathbf{0}$, the solution of the boundary value problem simplifies to

  $$\Phi(\vartheta) = \mathrm{e}^{\tilde{\lambda}\vartheta}\Delta^{-1}(\tilde{\lambda})\Psi_0. \tag{C45}$$

  This occurs in case of all the other coefficients of the SSM.

Appendix D Projection of a sampled trajectory

Assume that a trajectory $\mathbf{x}(t)$ is sampled with the sampling time $\Delta t = \tau/r$, where the integer r is the sampling delay number. Then, the sampled state vector takes the form

$$\mathbf{y}(k) = \begin{bmatrix} \mathbf{x}(t_k) \\ \mathbf{x}(t_{k-1}) \\ \vdots \\ \mathbf{x}(t_{k-r}) \end{bmatrix}, \tag{D46}$$

where $t_k = k\Delta t$ is the k-th sampling instant.

The projection of a trajectory to an eigenfunction $\mathbf{s}_j(\vartheta)$ is defined in (20); its discretized form assumes

$$y_j(k) = \mathbf{p}_j\left(\mathbf{x}(t_k) + \sum_{l=1}^{r}\mathbf{R}\mathrm{e}^{\lambda_j(l-r)\Delta t}\mathbf{x}(t_{k-l})\Delta t\right). \tag{D47}$$

The corresponding right-hand side can be rewritten in the form of the mapping

$$y_j(k) = \mathbf{T}_j\mathbf{y}(k), \tag{D48}$$

where

$$\mathbf{T}_j = \left[\mathbf{p}_j,\ \mathbf{p}_j\mathbf{R}\mathrm{e}^{\lambda_j(1-r)\Delta t}\Delta t,\ \ldots,\ \mathbf{p}_j\mathbf{R}\Delta t\right]. \tag{D49}$$

In this paper, when we referred to transformed trajectories, we meant that after this projection. We also subtracted that part of the trajectory, which is in the direction of the eigenfunction(s). This way, the corresponding SSM has a horizontal tangent space and the convergence of the trajectories is better visualized.

Assume that $\mathbf{s}(\vartheta)$ is a real eigenfunction, to which the projection is carried out. Then, the transformed trajectory $\tilde{\mathbf{x}}(t_k)$ assumes the form

$$\tilde{\mathbf{x}}(t_k) = \mathbf{x}(t_k) - y(t_k)\mathbf{s}(0). \tag{D50}$$

Similarly, complex conjugate eigenfunctions yield

$$\tilde{\mathbf{x}}(t_k) = \mathbf{x}(t_k) - y(t_k)\mathbf{s}(0) - \overline{y}(t_k)\overline{\mathbf{s}}(0). \tag{D51}$$

Note that the above described discrete time representation of DDEs is closely related to the delay embedding, which is a useful method to identify system parameters from data [68–70]; moreover, it is also applied in the SSMLearn package [20,71]. Delay embedding for ODEs allows one to create an observable vector that contains the state variables (or the combination of those) in subsequent time instances. This way, one obtains an extended state vector. Although, the coordinate on the SSM at time t depends only on the solution at time t, this is true for each time instance. Thus, delay embedding increases the number of equations in the regression analysis making it more accurate and less sensitive to noise.

In the above mentioned paper [71], the Vandermonde matrix, the range of which spans the tangent space of the SSM at the fixed point, has the same shape as the discretized eigenvectors of the delayed SSM calculation. Note that the left eigenvectors differ, since the orthogonality conditions are defined differently for ODEs and DDEs.

Applying delay embedding for delay differential equations, one should keep in mind that the τ long history is also relevant [70]. This results in the fact that while the depth of the embedding is preferred to be short in the case of ODEs, in the case of DDEs, this depth should be as long as the time delay of the system requires.

References

1. Davies, E.B.: Spectral theory and differential operators, vol. 42. Cambridge University Press, Cambridge (1995)
2. Rosenberg, R.: On nonlinear vibrations of systems with many degrees of freedom. Adv. Appl. Mech. **9**, 155–242 (1966)
3. Rand, R.H.: A direct method for non-linear normal modes. Int. J. Non-Linear Mech. **9**(5), 363–368 (1974)
4. Caughey, T., Vakakis, A.: A method for examining steady state solutions of forced discrete systems with strong nonlinearities. Int. J. Non-Linear Mech. **26**(1), 89–103 (1991)
5. Vakakis, A.F.: Ph.D. Dissertation, Analysis and Identification of Linear and Nonlinear Normal Modes in Vibrating Systems. California Institute of Technology, Pasadena (1991)
6. Shaw, S.W., Pierre, C.: Normal modes for non-linear vibratory systems. J. Sound Vib. **164**(1), 85–124 (1993)
7. Guckenheimer, J., Holmes, P.: Nonlinear oscillations, dynamical systems, and bifurcations of vector fields, vol. 42. Springer, New York (2013)
8. Lyapunov, A.M.: The general problem of the stability of motion. Int. J. Control **55**(3), 531–534 (1992)
9. Kelley, A.: On the Liapounov subcenter manifold. J. Math. Anal. Appl. **18**(3), 472–478 (1967)
10. Cirillo, G.I., Mauroy, A., Renson, L., Kerschen, G., Sepulchre, R.: A spectral characterization of nonlinear normal modes. J. Sound Vib. **377**, 284–301 (2016)
11. Haller, G., Ponsioen, S.: Nonlinear normal modes and spectral submanifolds: existence, uniqueness and use in model reduction. Nonlinear Dyn. **86**, 1493–1534 (2016)
12. Haro, A., Llave, R.: A parameterization method for the computation of invariant tori and their whiskers in quasi-periodic maps: rigorous results. J. Differ. Equs. **228**(2), 530–579 (2006)
13. Cabré, X., Fontich, E., Llave, R.: The parameterization method for invariant manifolds I: manifolds associated to non-resonant subspaces. Indiana Univ. Math. J. **52**, 283–328 (2003)
14. Cabré, X., Fontich, E., Llave, R.: The parameterization method for invariant manifolds II: regularity with respect to parameters. Indiana Univ. Math. J. **52**, 329–360 (2003)
15. Cabré, X., Fontich, E., De La Llave, R.: The parameterization method for invariant manifolds III: overview and applications. J. Differ. Equs. **218**(2), 444–515 (2005)
16. Szalai, R., Ehrhardt, D., Haller, G.: Nonlinear model identification and spectral submanifolds for multi-degree-of-freedom mechanical vibrations. Proc. Royal Soc. A **473**(2202), 20160759 (2017)
17. Breunung, T., Haller, G.: Explicit backbone curves from spectral submanifolds of forced-damped nonlinear mechanical systems. Proc. Royal Soc. A **474**(2213), 20180083 (2018)
18. Jain, S., Haller, G.: How to compute invariant manifolds and their reduced dynamics in high-dimensional finite element models. Nonlinear Dyn. **107**(2), 1417–1450 (2022)
19. Ponsioen, S., Pedergnana, T., Haller, G.: Automated computation of autonomous spectral submanifolds for nonlinear modal analysis. J. Sound Vib. **420**, 269–295 (2018)
20. Cenedese, M., Axås, J., Bäuerlein, B., Avila, K., Haller, G.: Data-driven modeling and prediction of non-linearizable dynamics via spectral submanifolds. Nat. Commun. **13**(1), 872 (2022)
21. Takens, F.: Detecting strange attractors in turbulence. In: Dynamical Systems and Turbulence. Warwick 1980: Proceedings of a Symposium Held at the University of Warwick vol. 1979(80), pp. 366–381. Springer, Berlin (1981)
22. Vizzaccaro, A., Shen, Y., Salles, L., Blahoš, J., Touzé, C.: Direct computation of nonlinear mapping via normal form for reduced-order models of finite element nonlinear structures. Comput. Methods Appl. Mech. Eng. **384**, 113957 (2021)
23. Opreni, A., Vizzaccaro, A., Frangi, A., Touzé, C.: Model order reduction based on direct normal form: application to large finite element MEMS structures featuring internal resonance. Nonlinear Dyn. **105**(2), 1237–1272 (2021)
24. Vizzaccaro, A., Opreni, A., Salles, L., Frangi, A., Touzé, C.: High order direct parametrisation of invariant manifolds for model order reduction of finite element structures: application to large amplitude vibrations and uncovering of a folding point. Nonlinear Dyn. **110**, 525–571 (2022)
25. Opreni, A., Vizzaccaro, A., Touzé, C., Frangi, A.: High-order direct parametrisation of invariant manifolds for model order reduction of finite element structures: application to generic forcing terms and parametrically excited systems. Nonlinear Dyn. **111**(6), 5401–5447 (2023)
26. Stoychev, A.K., Römer, U.J.: Failing parametrizations: what can go wrong when approximating spectral submanifolds. Nonlinear Dyn. **111**(7), 5963–6000 (2023)
27. Kogelbauer, F., Haller, G.: Rigorous model reduction for a damped-forced nonlinear beam model: an infinite-dimensional analysis. J. Nonlinear Sci. **28**, 1109–1150 (2018)
28. Buza, G.: Spectral submanifolds of the Navier–Stokes equations. SIAM J. Appl. Dyn. Syst. **23**(2), 1052–1089 (2024)
29. Hale, J.K., Verduyn Lunel, S.M.: Introduction to functional differential equations, vol. 99. Springer, New York (1993)
30. Stepan, G.: Retarded dynamical systems: stability and characteristic functions. Longman Scientific & Technical, New York (1989)
31. Mäkilä, P., Partington, J.: Shift operator induced approximations of delay systems. SIAM J. Control. Optim. **37**(6), 1897–1912 (1999)
32. Insperger, T., Stepan, G.: Semi-discretization for time-delay systems: stability and engineering applications, vol. 178. Springer, New York (2011)
33. Michiels, W., Jarlebring, E., Meerbergen, K.: Krylov-based model order reduction of time-delay systems. SIAM J. Matrix Anal. Appl. **32**(4), 1399–1421 (2011)
34. Farkas, G.: Unstable manifolds for RFDEs under discretization: the Euler method. Comput. Math. Appl. **42**(8–9), 1069–1081 (2001)

35. Sahai, T., Vladimirsky, A.: Numerical methods for approximating invariant manifolds of delayed systems. SIAM J. Appl. Dyn. Syst. **8**(3), 1116–1135 (2009)
36. Jarlebring, E., Damm, T., Michiels, W.: Model reduction of time-delay systems using position balancing and delay Lyapunov equations. Math. Control Signals Syst. **25**, 147–166 (2013)
37. van de Wouw, N., Michiels, W., Besselink, B.: Model reduction for delay differential equations with guaranteed stability and error bound. Automatica **55**, 132–139 (2015)
38. Scarciotti, G., Astolfi, A.: Model reduction of neutral linear and nonlinear time-invariant time-delay systems with discrete and distributed delays. IEEE Trans. Autom. Control **61**(6), 1438–1451 (2015)
39. Groothedde, C.M., James, J.M.: Parameterization method for unstable manifolds of delay differential equations. J. Comput. Dyn. **4**(1&2), 21–70 (2017)
40. He, X., Llave, R.: Construction of quasi-periodic solutions of state-dependent delay differential equations by the parameterization method I: Finitely differentiable, hyperbolic case. J. Dyn. Diff. Equat. **29**, 1503–1517 (2017)
41. He, X., Llave, R.: Construction of quasi-periodic solutions of state-dependent delay differential equations by the parameterization method II: Analytic case. J. Differ. Equs. **261**(3), 2068–2108 (2016)
42. Clément, P., Diekmann, O., Gyllenberg, M., Heijmans, H., Thieme, H.: Perturbation theory for dual semigroups I. The sun-reflexive case. Mathematische Annalen **277**(4), 709–725 (1987)
43. Clément, P., Diekmann, O., Gyllenberg, M., Heijmans, H., Thieme, H.: Perturbation theory for dual semigroups II. Time-dependent perturbations in the sun-reflexive case. Proc. Royal Soc. Edinburgh Sect. A **109**(1–2), 145–172 (1988)
44. Diekmann, O., Van Gils, S.A., Verduyn Lunel, S.M., Walther, H.-O.: Delay equations: functional-, complex-, and nonlinear analysis, vol. 110. Springer, New York (1995)
45. Wage, B.: Normal Form Computations for Delay Differential Equations in DDE-BIFTOOL. Master's thesis, Universiteit Utrecht, the Netherlands (2014)
46. Molnar, T.G., Insperger, T., Stepan, G.: Closed-form estimations of the bistable region in metal cutting via the method of averaging. Int. J. Non-Linear Mech. **112**, 49–56 (2019)
47. Molnar, T.G., Dombovari, Z., Insperger, T., Stepan, G.: On the analysis of the double hopf bifurcation in machining processes via centre manifold reduction. Proc. Royal Soc. A: Math., Phys. Eng. Sci. **473**(2207), 20170502 (2017)
48. Lelkes, J., Kalmar-Nagy, T.: Bifurcation analysis of a forced delay equation for machine tool vibrations. Nonlinear Dyn. **98**(4), 2961–2974 (2019)
49. Takacs, D., Orosz, G., Stepan, G.: Delay effects in shimmy dynamics of wheels with stretched string-like tyres. Eur. J. Mech.-A/Solids **28**(3), 516–525 (2009)
50. Beregi, S., Takacs, D., Stepan, G.: Bifurcation analysis of wheel shimmy with non-smooth effects and time delay in the tyre-ground contact. Nonlinear Dyn. **98**(1), 841–858 (2019)
51. Veraszto, Z., Stepan, G.: Nonlinear dynamics of hardware-in-the-loop experiments on stick-slip phenomena. Int. J. Non-Linear Mech. **94**, 380–391 (2017)
52. Habib, G., Bartfai, A., Barrios, A., Dombovari, Z.: Bistability and delayed acceleration feedback control analytical study of collocated and non-collocated cases. Nonlinear Dyn. **108**(3), 2075–2096 (2022)
53. Szaksz, B., Stepan, G.: Delay-induced bifurcations in collocated position control of an elastic arm. Nonlinear Dyn. **107**(2), 1611–1622 (2022)
54. Milton, J., Cabrera, J.L., Ohira, T., Tajima, S., Tonosaki, Y., Eurich, C.W., Campbell, S.A.: The time-delayed inverted pendulum: implications for human balance control. Chaos: An Interdiscip. J. Nonlinear Sci. **19**(2), 026110 (2009)
55. Molnar, C.A., Zelei, A., Insperger, T.: Estimation of human reaction time delay during balancing on balance board. In: 2017 13th IASTED International Conference on Biomedical Engineering (BioMed), pp. 176–180 (2017). IEEE
56. Zhang, L., Stepan, G., Insperger, T.: Saturation limits the contribution of acceleration feedback to balancing against reaction delay. J. R. Soc. Interface **15**(138), 20170771 (2018)
57. Orosz, G., Stepan, G.: Subcritical Hopf bifurcations in a car-following model with reaction-time delay. Proc. Royal Soc. A **462**(2073), 2643–2670 (2006)
58. Molnár, T.G., Orosz, G.: Destroying phantom jams with connectivity and automation: Nonlinear dynamics and control of mixed traffic. Transportation Science **published online** (2024)
59. Kravanja, P., Barel, M.: Computing the zeros of analytic functions. Springer, New York (2000)
60. Vyhlídal, T.: Analysis and Synthesis of Time Delay System Spectrum. Ph.D. thesis, Czech Technical University in Prague, Prague (2003)
61. Engelborghs, K., Luzyanina, T., Roose, D.: Numerical bifurcation analysis of delay differential equations using DDE-BIFTOOL. ACM Trans. Math. Softw. (TOMS) **28**(1), 1–21 (2002)
62. Breda, D., Maset, S., Vermiglio, R.: Computing the characteristic roots for delay differential equations. IMA J. Numer. Anal. **24**(1), 1–19 (2004)
63. Verheyden, K., Luzyanina, T., Roose, D.: Efficient computation of characteristic roots of delay differential equations using LMS methods. J. Comput. Appl. Math. **214**(1), 209–226 (2008)
64. Michiels, W., Niculescu, S.-I.: Stability and stabilization of time-delay systems: an eigenvalue-based approach. SIAM, Philadelphia (2007)
65. Kuznetsov, Y.A.: Elements of applied bifurcation theory, vol. 112. Springer, New York (1998)
66. Hassard, B.D., Kazarinoff, N.D., Wan, Y.-H.: Theory and applications of Hopf Bifurcation, vol. 41. Cambridge University Press, Cambridge (1981)
67. Sieber, J., Engelborghs, K., Luzyanina, T., Samaey, G., Roose, D.: DDE-BIFTOOL manual-bifurcation analysis of delay differential equations. arXiv preprint, arXiv:1406.7144 (2014)

68. Juang, J.-N., Pappa, R.S.: An eigensystem realization algorithm for modal parameter identification and model reduction. J. Guid. Control. Dyn. **8**(5), 620–627 (1985)
69. Williams, M.O., Kevrekidis, I.G., Rowley, C.W.: A data-driven approximation of the Koopman operator: extending dynamic mode decomposition. J. Nonlinear Sci. **25**, 1307–1346 (2015)
70. Ge, J.I., Orosz, G.: Connected cruise control among human-driven vehicles: experiment-based parameter estimation and optimal control design. Transp. Res. Part C **95**, 445–459 (2018)
71. Axås, J., Haller, G.: Model reduction for nonlinearizable dynamics via delay-embedded spectral submanifolds. Nonlinear Dyn. **111**(24), 22079–22099 (2023)